Interrelations between surface, boundary layer, and columnar aerosol properties derived in summer and early autumn over a continental urban site in Warsaw, Poland

Dongxiang Wang[1], Dominika Szczepanik[1], Iwona S. Stachlewska[1]

[1]Institute of Geophysics, Faculty of Physics, University of Warsaw, Warsaw, 02-093, Poland

Correspondence to: Iwona S. Stachlewska (iwona.stachlewska@fuw.edu.pl)

Abstract. PollyXT Raman Polarization Lidar observations were performed at the Remote Sensing Laboratory (RS-Lab) in Warsaw (52.2109°N, 20.9826°E), Poland, in the framework of the European Aerosol Research Lidar Network (EARLINET) and the Aerosol, Clouds and Trace gases Research Infrastructure (ACTRIS). Data collected in July, August and September of 2013, 2015 and 2016 were analysed using the classical Raman approach. In total 246 sets of intact profiles, each set comprising particle extinction (α) and backscatter coefficients (β) and linear particle depolarization ratios (δ) at 355 nm and 532 nm, were derived for statistical investigations and stored in the EARLINET/ACTRIS Data Base. The main analysis was focused on intensive optical properties obtained within atmospheric boundary layer (ABL). Their interrelations were discussed for different periods: entire day, nighttime (with respect to NL nocturnal and RL residual layer), at sunrise (MTL morning transition layer), and from late afternoon till sunset (WML well-mixed layer). Within boundary layer, the lidar derived optical properties (entire day, 246 sets) revealed the mean aerosol optical depth (AOD_{ABL}) of 0.20 ± 0.10 at 355 nm and 0.11 ± 0.06 at 532 nm; the mean Ångström exponent ($\text{Å}E_{ABL}$) of 1.54 ± 0.37; the mean lidar ratio (LR_{ABL}) of 48 ± 17 sr at 355 nm and 41 ± 15 sr at 532 nm; the mean linear particle depolarization ratio (δ_{ABL}) of 0.02 ± 0.01 at 355 nm and 0.05 ± 0.01 at 532 nm, and the mean water vapour mixing ratio (WV_{ABL}) of 8.28 ± 2.46 g/kg. In addition, the lidar derived daytime boundary layer optical properties (for MTL and WML) were compared with the corresponding daytime columnar aerosol properties derived from the shadowband radiometer MFR-7 measuring within the National Aerosol Research Network (PolandAOD-NET) and the sunphotometer CE318 of the Aerosol Robotic NETwork (AERONET). A high linear correlation of columnar aerosol optical depth of the two latter instruments operated in Warsaw was obtained (correlation coefficient of 0.98 with standard deviation of 0.02). A contribution of the aerosol load in the summer and early autumn free troposphere can result in a twice higher AOD_{CL} than AOD_{ABL} over Warsaw. Occurrence of turbulence driven aerosol burst from the boundary layer into the free troposphere can further increase this difference. Aerosol within ABL and in the free troposphere was interpreted based on comparisons of the properties derived at different altitude with the values reported in literature, so as characteristic for different aerosol, in a combination with the backward trajectories calculations, satellite data and models outputs. Within the boundary layer, it consisted either of urban anthropogenic pollution (~ 61%) or its mixtures with biomass burning aerosol (< 14%), local pollen (< 7%) or arctic marine particles (< 5%). No significant contribution of mineral dust in the boundary layer was found. The lidar derived atmospheric boundary layer height (ABLH) and AOD_{ABL} exhibited a

positive correlation (R of 0.76), associated with the local anthropogenic pollution (this being most pronounced for RL and WML). A positive correlation of AOD_{ABL} and LR_{ABL} and a negative correlation of $ÅE_{ABL}$ and LR_{ABL}, as well as the expected negative trends for WV_{ABL} (and surface relative humidity RH) and δ_{ABL}, were observed. Relations of the lidar derived aerosol properties within ABL and the surface in-situ measurements of particulate matter with an aerodynamic diameter < 10μm (PM_{10}) and < 2.5μm ($PM_{2.5}$) measured by Warsaw Regional Inspectorate of Environmental Protection (WIOS) Network, and the fine to coarse mass ratio (FCMR) were investigated. FCMR and surface RH showed positive correlation (R of 0.71 for MTL, 0.63 for WML and 0.6 for NL, respectively), what was seen even for nighttime - generally lacking statistically significant relations. A weak negative correlation of FCMR and δ_{ABL} (more pronounced at 532 nm, nighttime) and no casual relation between FCMR and $ÅE_{ABL}$ was found. Most interesting and distinct differences were observed for the morning transition layer (MTL) and the well-mixed layer (WML). The MTL was ranging up to 0.6-1 km, and was characterised by the lower AOD_{ABL} < 0.12, more wet conditions RH 50-80 %, smaller particles ($ÅE_{ABL}$ of 1-2.2; FCMR from 0.5 to 3), and the low LR_{ABL} of 20-40 sr. The WML was ranging up to 1-2.5 km and exhibited the higher AOD_{ABL} reaching up to 0.45, drier conditions RH 25-60 %, larger particles ($ÅE_{ABL}$ of 0.8-1.7; FCMR of 0.2-1.5), and the higher LR_{ABL} up to 90 sr.

Keywords: lidar; atmospheric boundary layer; aerosol optical properties; particulate matter; near-surface relative humidity,

1 Introduction

Atmospheric aerosol can impact climate (e.g. Feingold et al., 2016; Seinfeld et al., 2016), weather (e.g. Fan et al., 2016; Gayatri et al., 2017), air quality (e.g. Fuzzi et al., 2015) and human health (e.g. Zheng et al., 2015; Trippetta et al., 2016). Aerosol particles affect the Earth's radiative budget, as they interact with the incoming solar short-wave radiation and the outgoing terrestrial long-wave radiation. Depending on the aerosol type, they can scatter and/or absorb the radiation, thus causing warming or cooling of the atmosphere locally, at the surface, and at the top of atmosphere (Kaufman et al., 2002). The variety of aerosol sources, those of natural and anthropogenic origin, as well as the influence of diverse meteorological conditions on their characteristics and transport, lead to aerosol contents strongly variable within the troposphere. Aerosol optical properties, size and composition are important for aerosol-cloud-radiation interaction studies (Seinfeld et al., 2016) and for radiative transfer modelling (Lolli et al., 2018).

The Inter-governmental Panel on Climate Change (IPCC) reported that the sparse and/or poorly-known information on the aerosol temporal and spatial variability causes high uncertainty in the assessment of their influence on the global radiation budget (Stocker et al., 2013). The latest IPCC report indicates that the reduction of uncertainties is still needed, as it can improve the ability of accurate forecasts of global climate change (Masson-Delmotte et al., 2018). Several studies were dedicated to investigate and improve the mentioned uncertainties. Pan et al. (2015) identified the major discrepancies between the state-of-the-art global aerosol models and observations in simulating aerosol loading over South Asia, thus providing directions for future model improvements in this important region. Ghan et al. (2016) found that uncertainty in anthropogenic aerosol effects on cloud

radiative forcing arises from uncertainty in several relationships, a.o. the choice of parameter values and numerical integration methods. Koffi et al. (2016) provided further spatial and temporal details on the state-of-the-art AeroCom II global aerosol models and investigated the reasons for the model discrepancies and diversity, which is laying a good base for further evaluating the models' performance at a global scale. Kipling et al. (2016) investigated the impact of a wide range of processes (emission,

5 transport, deposition, microphysical and chemical processes) on aerosol vertical distribution in the HadGEM3− UKCA aerosol–climate model through a series of limiting case process-based sensitivity tests, whereby they showed that the processes, which have the greatest impact on the vertical distribution vary both between different aerosol components and over the particle size spectrum. Seinfeld et al. (2016) provided strategies for improving estimates of aerosol−cloud relationships in climate models, for new remote sensing and in situ measurements, and for quantifying and reducing the model uncertainties.

10 Air pollution is one of the major environmental issues in metropolitan areas due to its adverse effects on human health (e.g. Chen et al., 2008; Lelieveld et al., 2015). Juda-Rezler et al. (2012) reported that air quality is related to anthropogenic emissions and natural emissions, whereby the change of temperature, water vapor, precipitation, wind speed and wind direction can affect atmospheric chemical reactions, atmospheric transport and deposition processes, as well as the rate of pollutant transport from urban environments to global scale environments. The emissions of pollutants change the chemical composition of the

15 atmosphere, which in turn has a feedback effect on the regional and global climate (Juda-Rezler et al., 2012). Strong emissions, e.g., from traffic, industry or heating, can drastically decrease air quality, particularly when meteorological conditions prevent an exchange of polluted and clean air, (Juda-Rezler et al., 2011). In Europe, surface particulate matter with an aerodynamic diameter below 10μm (PM_{10}) and 2.5μm ($PM_{2.5}$) is one of the most serious air quality problems (e.g. De Leeuw et al., 2001; Wolff and Perry, 2010). As atmospheric aerosol can affect air quality, health and environment, joint studies of the aerosol optical properties

20 measurements in a combination with the surface observations of PM_{10} (e.g. Guo et al., 2009; 2017; Stachlewska et al., 2017b; Popovici et al., 2018), $PM_{2.5}$ (e.g. Schaap et al., 2009; Stachlewska et al., 2017b; 2018) and PM_1 (e.g. Qin et al., 2018) concentrations can improve our knowledge on atmospheric environment.

The atmospheric boundary layer (ABL) can affect the dispersion of pollutants within the mixing layer (Wałaszek et al., 2018). The knowledge on atmospheric boundary layer characteristics and its dynamics, both related to ambient meteorological conditions, is

25 helpful to model and predict mechanisms that matter in weather forecasting, air pollution and climate change studies (Barlage et al., 2016). Therefore, it is meaningful to acquire the knowledge of the ABL top height distribution along with the aerosol optical properties within the ABL.

Lidar techniques seem to be an optimal tool to provide height-resolved aerosol data products. Several lidar techniques suitable for aerosol studies matured recently. In the last ten years, a rapid progress in the laser technology, measurement techniques, and data

30 acquisition systems has contributed to a much wider use of these techniques also for the aerosol monitoring, ranging from the simple elastic backscatter lidar / ceilometer networks (Flentje et al., 2010; Lolli and Di Girolamo, 2015) to the most advanced multi-wavelength Raman lidar system networks (Baars et al., 2016). The European Aerosol Research Lidar Network (EARLINET; https://www.earlinet.org) conducts lidar observations and provides relevant sets of lidar data products stored in a comprehensive, quantitative, and statistically significant database for the aerosol distribution over Europe (Pappalardo et al.,

2014). Quality assurance program (Freudenthaler et al., 2018) and lidar data evaluation algorithms (Böckmann et al., 2004) have been developed and assessed at each lidar station, as well as during the lidar intercomparison campaigns (e.g. Wandinger et al., 2016) to meet accuracy standards desired in aerosol radiative forcing need. The unique data set of lidar observations conducted over Europe allows for classification of the aerosol type (e.g. Nicolae et al., 2018; Papagiannopoulos et al., 2018). The

5   EARLINET network is an integral part of the Aerosol, Clouds and Trace gases Research Infrastructure (ACTRIS; https://www.actris.eu) - a pan-European initiative consolidating actions amongst European partners producing high-quality observations of aerosol, clouds and trace gases. As different atmospheric processes are increasingly in the focus of many societal and environmental challenges, such as air quality, health, sustainability and climate change, ACTRIS initiatives aim at contributing to resolving of challenges by providing a platform for researchers to combine their efforts more effectively, and by

10   providing observational data of aerosol, clouds and trace gases openly to other external users.

The aerosol optical properties derived for boundary layer from lidar have been studied in a statistical approach at several EARLINET sites in Europe (e.g. Matthias et al., 2004; Mattis et al., 2004; Amiridis et al., 2005; Sicard et al., 2011; Siomos et al., 2018). However, most of these studies were restricted to analysis of either AOD and/or LR values in ABL (e.g. Matthias et al. 2004; Amiridis et al. 2005, 2009; Sicard et al., 2011), or relations between LR_{ABL} and AE_{ABL} (Giannakaki et al., 2010). The

15   comprehensive investigations of interrelations of various aerosol optical properties were not reported in the past. The current study is the first that reports on their interrelations (or lack of it) for different time of day (nocturnal time, sunrise and sunset, daytime) in summer (July and August) and early autumn (September) over Warsaw. The relations of surface $PM_{2.5}$, PM_{10} and AOD_{CL} were reported by e.g. Guo et al., 2009; Filip and Stefan, 2011; Zang et al., 2017; Szczepanik and Markowicz, 2018 and the relations of AOD_{CL} and ambient RH were reported by e.g. Bergin et al., 2000; Altaratz et al., 2013. Stachlewska et al. (2017b; 2018),

20   investigated the relations of $PM_{2.5,}$ $PM_{10,}$ RH and LR_{ABL}, AOD_{ABL}, AE_{ABL}, $δ_{ABL,}$ based on the case studies. In this paper, we analyse and report on the latter based on long-term observations. Combination of such study with hygroscopic growth monitoring is the next step in the future (Navas Guzmán et al., 2019). The results reported in the current paper shall enrich the state of knowledge on boundary layer aerosol optical properties by building a seasonal climatology over Warsaw (even if limited to July-September of the 3-years period) and thus, to provide a reference for comparative studies with the other EARLINET sites (e.g.

25   Papayannins et al., 2008) and AERONET sites (e.g. Siomos et al., 2018). The obtained data set has an excellent potential for the aerosol microphysical parameters inversion (e.g. Veselovskii et al., 2002; Böckmann et al., 2005) and can be used also for testing the aerosol typing algorithms (e.g. Nicolae et al., 2018; Papagiannopoulos et al., 2018). This research provides parameters for studies of boundary layer meteorology and the derived aerosol optical properties can serve for verification of aerosol transport models (e.g. Binietoglou et al., 2015), it can be used in estimation of aerosol radiative forcing effect in radiative transfer modelling

30   (e.g. Lisok et al., 2018, Lolli et al., 2018), as well as utilized in validation of space-borne lidar (e.g. Illingworth et al., 2015; Papagiannopoulos et al. 2016; Proestakis et al. 2019).

In the framework of the EARLINET, extensive observations at a continental, urban site in Warsaw at the Remote Sensing Laboratory (RS-Lab) of the Institute of Geophysics at the Faculty of Physics at the University of Warsaw have been performed since July 2013. Within the current paper the data products of Warsaw site published in the EARLINET/ACTRIS Data Base were

utilized (The EARLINET Publishing Group, 2018). The study was dedicated to calculations and analysis of the aerosol optical properties derived within the atmospheric boundary layer, at various times of day, during summer (July and August) and early autumn (September) in the years of 2013, 2015 and 2016, over a continental urban site in Warsaw. The three specific goals were addressed: i) an investigation of interrelations between the different aerosol optical properties, ii) an investigation of relations between the aerosol optical properties, particulate matter ($PM_{2.5}$ and PM_{10}) and the relative humidity, and iii) an assessment of the quantitative contribution of the boundary aerosol optical depth into the columnar aerosol optical depth. In section 2, the instrumentation and datasets are described. Section 3 presents methodology of boundary layer height derivation and the aerosol optical properties retrieval approaches. Section 4 focuses on comparisons of different types of mean optical properties as derived within boundary layer and in the atmospheric column, PMs, ABLHs and near-surface relative humidity. Conclusions are given in section 5.

2 Instrumentation and data set

The Raman polarization and water-vapor lidar (52.2109°N, 20.9826°E, 112 m a.s.l.) is located at the Remote Sensing Laboratory (RS-Lab, https://www.igf.fuw.edu.pl/en/instruments) of the Institute of Geophysics at the Faculty of Physics of the University of Warsaw, Poland. Location of the RS-Lab is denoted in Figure 1. The RS-Lab conducts observations as a part of the European Aerosol Research Lidar Network (EARLINET, www.earlinet.org, Pappalardo et al., 2014), it provides regular measurements within the worldwide Polly.NET lidar network (http://polly.tropos.de/, Baars et al., 2016) and within the National Aerosol Research Network PolandAOD-NET (www.polandaod.pl , supplement material in Markowicz et al., 2016). The so-called NeXT generation PollyXT lidar deployed in Warsaw was described in a great detail in Engelmann et al (2016).

Since July 2013, PollyXT lidar performs quasi-continuous 24/7 observations. Powerful laser pulses (180, 110 and 60 mJ) at 1064, 532 and 355 nm are emitted co-axially and vertically, with a 20 Hz repetition frequency, into the atmosphere. Detection is performed with a Newtonian telescope at 8-channels (so-called $2\alpha+3\beta+2\delta+WV$), which enables determination of the particle extinction coefficient profiles (α) at 532 nm and 355 nm, the particle backscatter coefficient profiles (β) at 1064 nm, 532 nm and 355 nm, the linear particle depolarization ratio profiles (δ) at 532 and 355 nm, and the water vapour mixing ratio (WV). The signals at all channels are recorded up to 48 km with a standard 7.5 m vertical and 30 s temporal resolutions. Measured signals are affected by an incomplete geometrical overlap between the emitted laser beam and the receiving telescope, and therefore the signals in the range below 400 m altitude are rejected from further evaluation. The overlap-range issue posed a first constrain on the selected dataset, i.e. constraining analyses to the summer and early-autumn (July-September) data. In winter, the atmospheric boundary layer height derived at noon and midnight from the radiosounding profiles, was found often enough below the complete lidar's overlap range. Hence, in winter, within the range in which the divergent lidar laser beam is not fully received by the full field of view of the lidar telescope, the detection of the boundary layer height by lidar is limited. In contrast, in summer and early autumn, the boundary layer height is always above the complete lidar's overlap range, and thus it is not affecting the derived profiles. Therefore, we restricted the analyses of the optical properties within boundary layer to the latter period. Moreover, the

analysis was restricted to the complete sets of profiles of aerosol properties (i.e. $2\alpha+3\beta+2\delta+WV$) derived in 2013, 2015 and 2016, as for the named period, for this site, it was feasible to obtain the highest number of quality controlled lidar profiles. They were then calculated and stored in the EARLINET/ACTRIS Date Base. Although the PollyXT lidar in Warsaw performs quasi-continuous 24/7 observations, the data cannot be obtained on every single day. Unfavourable weather conditions (e.g.

5   precipitation or thick low-level clouds) significantly limit the number of observations in spring and late autumn, and practically prevent it in winter. Instrumental issues occur (e.g. technical failures), which are season independent but in some periods lasted several weeks or months. Finally, even if observations were performed, it was not always feasible to derive the aforementioned full sets of aerosol properties (e.g. due to too strong background light at daytime; too low (high) aerosol load). Note that, for the selected period of July-September of 2013, 2015 and 2016, there was no other site that provided such a high number of the

10   complete sets of measurements within the EARLINET Data Base.

Quality checked profiles of optical properties are stored in the EARLINET/ACTRIS Data Base (www.earlinet.org). The statistical analysis covers profiles derived for EARLINET regular measurements (Mondays and Thursdays with ± 2 hours from zenith and sunset) and for dedicated measurements (e.g. diurnal cycles, special alert events). From Warsaw site, only cloud-screened profiles evaluated using the classical Raman-approach are feed into the Data Base. The profiles obtained for lidar observations in July,

15   August and September in the year of 2013, 2015 and 2016 were analysed (2014 was excluded from analyses due to too sparse data availability). In total, 246 lidar profiles were collected for this study (denoted as contributing to *entire time*), whereby 113 profiles were obtained for *nocturnal time* (21:00-02:00 UTC) and 37 profiles were derived at sunrise (03:00-08:00 UTC) and 63 profiles at sunset (16:00-20:00 UTC), here defined as the *sunrise/sunset or transition time*. The precise sunrise and sunset times are available via www.timeanddate.com/sun/poland/warsaw. The analysed time is separated into three periods because the change of

20   atmospheric conditions is driven by different processes during those times, allowing therefore a possibility to search for and signature of aerosol optical properties change. Note, that only 29 profiles were available at daytime conditions (08:00-16:00 UTC), which was considered as too low number to consider separately the category of daytime, i.e. these profiles join the category entire time. However, comparisons of the optical properties derived from lidar and photometer were done for a subset of daytime profiles (03:00-19:00 UTC).

25   Multi-Filter Rotating Shadowband Radiometer (MFR-7; Yankee Environmental Systems) was used for continuous passive measurements at the RS-Lab in the frame of the PolandAOD-NET network activities. The instrument operates at six narrow-band channels (415, 500, 615, 673, 870 and 940 nm) and one broadband channel. It measures direct, diffuse and total solar radiation, from which the spectrally resolved aerosol optical depth is obtained. In-situ calibration using the classic Langley approach is applied on regular basis. Details on the instrument design and uncertainty analyses are reported in Harrison et al. (1994). Cloud-

30   screened products used in this study are: AOD_{CL} (415) and AOD_{CL} (500) with uncertainty at the level of ±0.025, and $\mathring{A}E_{CL}$ (415/500) with uncertainty at the level of ±0.04. There is a threshold on the values of $AOD_{CL} <0.03$, being excluded from analyses.

Sunphotometer (CE318; CIMEL Electronique) is operated at the Institute of Geophysics of the Polish Academy of Sciences (IGF-PAS) in the Observatory in Belsk (51.8366°N, 20.7916°E, 190 m a.s.l.), located 43.7 km south-west of the RS-Lab in Warsaw

providing longest record of passive measurements in Poland. The same instrument was recently installed in RS-Lab in Warsaw and since January 2018 provides data to the AERONET Date Base. Passive measurements of direct and diffuse solar irradiance and sky radiance at the Earth's surface at nine wavelengths in a spectral range from 340 nm to 1640 nm are used for retrieval of AOD and ÅE. The data are calibrated once a year at PHOTONS/AERONET-EUROPE calibration centre (http://loaphotons.univ-

5   lille1.fr) and processed by the Aerosol Robotic NETwork (AERONET, http://aeronet.gsfc.nasa.gov, Holben et al., 1998). The Version 3 products (Giles et al., 2019) of AERONET Level 2.0 cloud screened AOD_{CL}(380) and AOD_{CL}(500) with uncertainty at the level of ±0.01, and $ÅE_{CL}$(380/500) with uncertainty at the level of ±0.03 were used. There is a threshold on the values of AOD_{CL} <0.03, being excluded from analyses. Note that, the AOD_{CL} from MFR-7 and CE318 are scaled using the Ångström law (Ångström, 1929, Iqbal, 1983) to match either one another or the lidar wavelength. The sunphotometer, it is located about 2 km

10   from the village of Belsk, in a typical agricultural region with fertile soil and trees. Note that the AERONET data in Belsk were used in the current study only for data consistency check and only as an indicative that the free tropospheric aerosol load existed above Warsaw and in its vicinity, and therefore, sunphotometer data from Belsk do not contribute to the core results. Note that, the AERONET sunphotometer of the same kind is also operated (since January 2018) at the RS-Lab of the University of Warsaw. The data of the letter instrument, specifically intercomparison of AODs obtained with the collocated CE318 and MFR-7

15   instruments at the RS-Lab, constitute a vital part of the results.

Particulate matter concentrations for particles with an aerodynamic diameter of less than 2.5µm and 10µm (denoted $PM_{2.5}$ and PM_{10}, respectively) were measured at the air quality monitoring site of the Warsaw Regional Inspectorate of Environmental Protection (WIOS) in Warsaw-Ursynow, located 6.5 km from the RS-Lab. The daily and hourly averaged $PM_{2.5}$ and PM_{10} data are visualised via http://sojp.wios.warszawa.pl/raport-dobowy-i-roczny. The data measurements conducted at the stations of State

20   Environmental Monitoring are gathered in the Air-Quality database JPOAT 2,0 of the National Chief Inspectorate for Environmental Protection (GIOS). This official, calibrated datasets of $PM_{2.5}$ and PM_{10} are accessible via http://powietrze.gios.gov.pl/pjp/archive. The measurement uncertainty is below 30% for the hourly concentrations. Products used in this study: surface daily and hourly mean particulate matter concentrations for $PM_{2.5}$ and PM_{10}, and the fine-to-coarse mass ratio (FCMR) defined as $PM_{2.5}/(PM_{10}-PM_{2.5})$ (Zawadzka et al., 2013). FCMR > 1.5 denotes *fine particles* domination (diameter <

25   2.5µm); FCMR < 0.5 means *coarse particles* domination (diameter between 2.5 µm to 10 µm). Values in the range of 0.5 < FCMR< 1.5 indicate that fine and coarse particles are distributed approximately equally.

The temperature, pressure, relative humidity, wind speed, and direction at the surface (p, T, RH, V, Vdir), were measured by the weather transmitter WXT510 (Vaisala) mounted on the roof platform of the RS-Lab at 21 m above the ground's surface. The atmospheric pressure, temperature and relative humidity profiles are obtained from the radiosonde RS92 (Vaisala) launched at two

30   World Meteorological Organization sites located in Poland: WMO 12374 station in Legionowo (52.40°N, 20.96°E, 96 m a.s.l., 25 km North of Warsaw) and WMO 12425 station in Wroclaw (51.78°N, 16.88°E, 122 m a.s.l., 300 km South-West of Warsaw). The noon and midnight radiosounding profiles (launch at 11:15 / 23:15 UTC, duration of circa 1.5 h) were visualized and downloaded via the University of Wyoming Upper Air Data website (weather.uwyo.edu/upperair/sounding.html).

Note that the shadowband radiometer and the sunphotometer derived AOD and the in-situ measured PM concentration values are averaged with corresponding time of the lidar derived optical profiles available for given period for the Warsaw site in the EARLINET/ACTRIS Data Base. Moreover, MFR-7 and CE318 collected data only at daytime. The measurement sites are showed in Figure 1. The PM site is located in the residential area of Ursynow suburb. The RS-Lab is located at the University campus at Ochota suburb shrouded by green parks. Between the three sites in Warsaw-Ochota, Warsaw-Ursynow and Belsk, there are no industrial pollution sources and anthropogenic pollution in summertime is related to traffic (Zawadzka et al., 2013).

3 Methodology of lidar products retrieval

The atmospheric boundary layer is regarded as the lowest layer of the troposphere, being directly influenced by the Earth's surface and reacting quickly to the surface forcing (Stull. 1988). The atmospheric boundary layer height (ABLH) can be derived from the lidar elastic-scattering aerosol backscatter signal, relying on a higher aerosol load within the boundary layer than in the free troposphere. Dang et al. (2019) summarized recently available methods for the ABLH retrievals. The limitations and capabilities of mixing height retrieval algorithms for different lidar and ceilometer systems were investigated by Haeffelin et al. (2012). Comerón et al. (2013) discussed the wavelet correlation transform method and the gradient method for the determination of ABLH by lidar. Stachlewska et al. (2012) used the latter method for the first retrievals of ABLH in Warsaw. Wang et al. (2019) reported that for the PollyXT lidar data in Warsaw, the most optimal for ABLH retrieval is the wavelet covariance transform method (WCT). As for the WCT method applied in our study, the covariance transform W_f of the Haar wavelet function h, is defined as in Equation 1:

$$W_f(a,b) = \frac{1}{a}\int_{z_1}^{z_2} P(z)\cdot h\left(\frac{z-b}{a}\right)dz, \qquad h\left(\frac{z-b}{a}\right) = \begin{cases} +1 & b-\frac{a}{2}\leq z\leq b \\ -1 & b\leq z\leq b+\frac{a}{2} \\ 0 & elsewhere \end{cases} \tag{1}$$

where $P(z)$ is the lidar elastic signal, z_1 and z_2 are the lower and upper limits of the signal, z is the altitude, and a is the dilation and b is the centre of the Haar wavelet function. The WCT calculations were done with the dilation of 30 range-bins applied on signals averaged over 7.5 m and 30 min, and the ABLH was derived at all three elastic wavelength signals (355, 532 and 1064 nm), and then averaged for a final result.

Aerosol optical properties can be derived in different ways. The Cloud-Aerosol Lidar and Infrared Pathfinder Satellite can provide the range-resolved profiles of aerosol and clouds (Winker et al., 2007). The combined ground-based lidar and cloud radar is capable to obtain vertical structure of cloud and aerosol properties (e.g. Delanoë and Hogan, 2008). The High Spectral Resolution Lidar technique allows for the separation of molecular and aerosol signals (e.g. Grund and Eloranta, 1991; Burton et al., 2012). The aerosol and cloud information can be retrieved by Multi-wavelength Raman lidars (e.g. Müller et al., 2007; Giannakaki et al.,

2010; Alados-Arboledas et al., 2011; Baars et al., 2016; Lolli et al., 2018; Ansmann et al., 2018). The latter lidar technique was used for this study.

Lidar signals stored in the EARLINET/ACTRIS Data Base were evaluated using the classical Raman retrieval approach. The particle extinction coefficient profiles at 355 and 532 nm were calculated from the so-called Raman lidar equation using the Rayleigh law for molecules and the Ångström law (usually with ÅE=1) for aerosol particles. The particle extinction coefficient (α_p) was derived as in Equation 2:

$$\alpha_p = \frac{\dfrac{d}{dz}\left(\ln\left(\dfrac{N}{P_N z^2}\right)\right) - \alpha_{\lambda_0}^m - \alpha_{\lambda_N}^m}{1 + \left(\dfrac{\lambda_0}{\lambda_N}\right)^k} \tag{2}$$

where N denotes the molecular number density of the nitrogen, λ_0 the emitted wavelength (355 or 532 nm), λ_N the wavelength of the nitrogen channel (387 or 607 nm), P_N the Raman signal at the nitrogen channel, z the distance from the lidar, $\alpha_{\lambda_i}^m$ (i=0, N) the molecular extinction coefficient at the emitted or the nitrogen wavelength, and k the wavelength dependence of particle.

The particle backscatter coefficient profiles (β_p) at 355, 532 and 1064 nm are derived with the use of the obtained particle extinction coefficient profiles at 355 nm and 532 nm (used for both larger wavelengths) and calibrated at the height range free of aerosol. More details on the exact procedure is given in Baars et al. (2016).

The linear particle depolarization ratio (δ_p) was derived as the ratio of the cross channel and the corresponding total channel at the same wavelength, using Equation 3:

$$\delta_p = \frac{(1+\delta_m)\delta_v\left(1+\dfrac{\beta_p}{\beta_m}\right) - (1+\delta_v)\delta_m}{(1+\delta_m)\left(1+\dfrac{\beta_p}{\beta_m}\right) - (1+\delta_v)} \tag{3}$$

where, δ_v is the linear volume depolarization ratio, δ_m is the linear depolarization ratio of air molecules and β_m is the molecule backscatter coefficient. The procedure for the ±45 depolarization calibration is used as in Engelmann et al. 2016.

The water vapour mixing ratio (WV) was obtained as the ratio of the Raman water vapor channel and the Raman nitrogen channel, as described in Stachlewska et al. (2017a), using Equation 4:

$$WV = C\frac{P_{\lambda H2O}}{P_{\lambda N}}\exp\left(-\left(\alpha(\lambda_{H2O}) - \alpha(\lambda_N)\right)\right) \tag{4}$$

where, $P_{\lambda N}$ is the Raman backscatter signal of the nitrogen channel wavelength λ_N=387 nm, $P_{\lambda H2O}$ is the Raman backscatter signal of water vapor channel wavelength λ_N=407 nm, C is the calibration constant.

For all analysed data products, low- and mid-altitude clouds are screened prior to the retrieval. The profiles of δ_p, β_p and δ_p were averaged over 60 min (60%) or 45 min (23%) or 30 min (17% of profiles used), depending on the atmospheric conditions

variability and the signal-to-noise ratio. Iarlori et al. (2015) reported that smoothing procedures can affect the features of lidar signal profile. For the EARLINET/ACTRIS Date Base, we store the files with profiles smoothed with the running mean over 49 (b-file) and 101 (e-file) range-bins (length of the single range-bin is 7.5 m), found as optimal for the PollyXT lidar data products derived at the Warsaw site. Typically, the α_p profiles need higher smoothing than β_p and δ_p profiles. However, we keep two

5 versions of the smoothed profiles in the Data Base. In this paper, the profiles smoothed over 49 range-bins were used. Keeping the smoothing at the same level has an advantage not only for the error estimations and the profiles comparisons but also for the microphysical parameter inversion (Janicka et al., 2017). The profiles of the WV were averaged over 30-60 min and 60 m with no smoothing applied. In lidar retrieval, the atmospheric profiles obtained by radiosounding at Legionowo or Wroclaw were used depending on the approaching direction of the air-mass transport.

10 After having determined ABLH, the mean values of different optical properties within the boundary layer are derived. For the incomplete overlap region, a special care to the data in the lowermost altitude range had to be applied. The lowest value of available particle extinction coefficient was assumed as representative down to the ground surface; this being commonly accepted approach in lidar studies, e.g. Matthias et al. (2004). Therefore, the mean extinction coefficient of the entire ABL was obtained by extrapolating the extinction profile with this value down to the ground. Similarly, the mean backscattering coefficient and the

15 particle depolarization ratio of ABL were extrapolated. Although the δ profiles can be derived almost to the ground, for the EARLINET/ACTRIS Data Base profiles are stored only down to 400 m, so that extrapolation also here was required. The water vapour mixing ratio profiles were also extrapolated, from 100 m down to the ground. The WV profiles are calculated using the ratio of two signals at 407 and 387 nm Raman channels. The overlap term of those two channels (close in spectral range; only 20 nm) practically cancels when calculating their ratio. Similarly, for the particle depolarization ratio (cross and total ratio at the same

20 wavelength), the overlap term also cancels. Therefore, the water vapor (so as the depolarization ratio profile can be obtained almost down to the ground. The Water vapour nighttime detection in July-September is typically performed from 20:00 to 4:00 UTC, thus only the data corresponding to the nocturnal time (21:00 to 2:00 UTC) were analysed.

Within ABL, the vertical distribution of the lidar ratio (LR_{ABL}) was derived as a ratio of the aerosol extinction to backscatter coefficient profiles at 355 and 532 nm ($LR=\alpha_p/\beta_p$), and then the mean LR_{ABL} were calculated.

25 The vertical distribution of the Ångström exponent $\mathring{A}E_{ABL}$ (355/532) was computed by the means of using the profiles of aerosol extinction coefficient (not AOD) at 355 and 532 nm, then the mean $\mathring{A}E_{ABL}$ was calculated using Equation 5:

$$AE = -\frac{\ln\left(\frac{\alpha_p(\lambda_1)}{\alpha_p(\lambda_2)}\right)}{\ln\left(\frac{\lambda_1}{\lambda_2}\right)} \quad (5)$$

The aerosol optical depth within boundary layer (AOD_{ABL}) was calculated by integrating the extrapolated (to the ground) aerosol extinction profile at 355 and 532 nm, from the height of $z_1=0$ to the height of the boundary layer top $z_2=ABLH$, as in Equation 6:

$$AOD = \int_{z_1}^{z_2} \alpha_p dz \qquad (6)$$

There is a threshold set on the mean values of AOD_{ABL} (355) < 0.05 and AOD_{ABL} (532) < 0.03 within the lowermost 1 km, i.e. the aerosol extinction coefficient profiles are extrapolated according to the AOD threshold for each wavelength. If AOD within 1 km is below the threshold, re-extrapolation is applied from a range-bin just above the initially chosen one down to the ground in an iterative manner, until the AOD values within 1 km meet the given above thresholds.

Stachlewska et al. (2018) reported the uncertainty of AOD_{ABL} at 355 and 532 nm derived from the Raman extinction coefficient profiles < 20%, the uncertainty of LR_{ABL} derived by extinction-to-backscattering coefficient ratios at 355 and 532 nm < 35%, and the uncertainty of δ_{ABL} at 355 and 532 nm < 20% of derived value. The uncertainty of extinction-derived ÅE_{ABL} (355/532) is < 30%. The uncertainty of the ABLH retrieval from PollyXT lidar is of ±70 m (Wang et al., 2019).

Finally, we attempt to interpret the aerosol measured within the boundary layer during the specified observational period over Warsaw. A number of publications highlighted the aerosol studies with usage of backward trajectories to interpret the possible aerosol source/type based on optical properties of observed aerosol and on the origin of air-masses containing aerosol (e.g. Dörnbrack et al., 2010; Mona et al., 2012; Nemuc et al., 2014; Burton et al., 2015; Granados-Muñoz et al., 2015; Jung et al., 2016; Papagiannopoulos et al., 2016; Schmeisser et al., 2017; Szkop and Pietruczuk 2017; Ansmann et al., 2018; Di Biagio et al., 2018; Horvath et al., 2018; Foth et al., 2019). In this paper, it was done in a standard way, case by case, based on the aerosol optical properties (LR, δ, ÅE, RH) comparison with the values reported in literature (an excellent review of those is provided by e.g. by Nicolae et al., 2018), as well as by calculating the HYbrid Single-Particle Lagrangian Integrated Trajectory (HYSPLIT) trajectories (Stein et al., 2015). All of the 246 analysed profiles were checked against the 3-10 days backward trajectories obtained in the boundary layer and the free troposphere, starting at altitudes of 0.5, 1.2, and 3 km, applied on the Global Data Assimilation System (GDAS) and CDC1 meteorological data, (trajectories are available via the PolandAOD-NET website). We assessed possible source of aerosol by inspecting the trajectories and the aerosol optical properties against the satellite data (i.e. Moderate Resolution Imaging Spectroradiometer (MODIS); Spinning Enhanced Visible and Infrared Imager (SEVIRI); Cloud-Aerosol Lidar and Infrared Pathfinder Satellite Observations (CALIPSO)) and the model outputs (Navy Aerosol Analysis and Prediction System (NAAPS), http://www.nrlmry.navy.mil/aerosol), as described by Stachlewska et al. (2018).

Roughly speaking, LR > 75 sr can indicate an existence of aerosol particles related to biomass burning, 40-50 sr to mineral dust, 50-60 sr to anthropogenic pollution, and 20-30 sr to arctic marine particles, although those values are depicting an ideal case (a pure aerosol type barely exists) and the values superimpose for the different aerosol species, as it is indicated in Table 1.

Particle linear depolarization ratio (δ_p) can be used as a tracer of spherical and non-spherical particles, whereby, the low values of δ < 0.01 can be regarded as due to very small spherical particles (e.g. pollution), the values of 0.2 < δ < 0.35 as due to dust (polluted dust values are lower, down to even 0.1). Values 0.04 < δ < 0.08 can be regarded as characteristic for biomass burning aerosol, then for pollen ~ 0.1, and for urban pollution < 0.2. Also here, values can superimpose for the different aerosol species, as it is indicated in Table 1.

The Ångström exponent (ÅE) can be used as an indicator of the size of atmospheric aerosol particles. Values of ÅE $\leq$ 1 indicate particle size distribution dominated by the coarse-mode aerosol (radii $\geq$ 0.5 μm, here called *large particles*) that are typically associated with dust and sea salt particles (Perrone et al. 2014). Values of ÅE $\geq$ 1.5 indicate size distributions dominated by the fine-mode aerosol (radii < 0.5 μm, here called *small particles*) that are associated with urban pollution (Perrone et al. 2014). Values within the range of 1< ÅE < 1.5 belong to accumulation-mode (here called *medium-size particles*) and are associated with biomass burning aerosol (Janicka et al., 2017). Use of the ÅE nomenclature of *small, medium, and large* size particle is for clarity, as not to confuse them with the fine-to-coarse mass ratio (FCMR).

For brevity, hereafter the α_p, β_p and δ_p are denoted as α, β and δ.

4 Results and discussion

Table 2 shows the mean particle extinction coefficient (α), particle backscatter coefficient (β), aerosol optical depth (AOD), lidar ratio (LR), linear particle depolarization ratio (δ) and Ångström exponent (ÅE) derived at 355 and 532 nm channels within the atmospheric boundary layer (ABL) for the entire (ET), nocturnal (NT) and transition (TT) time obtained for the measurement period of July-September of 2013, 2015, and 2016. Different mechanisms govern the sunrise and sunset conditions; the first is driven by the development of the convective boundary layer; the latter, lessens the convection to prone stratification with the residual layer (RL). Thus, the developed ABLH algorithm determines the atmospheric boundary layer top as a morning transition layer (MTL), a well-mixed layer (WML), a nocturnal layer (NL) and/or a residual layer (RL).

The mean entire time (24h) ABLH was of 1.33±0.36 km for July-September of 2013, 2015 and 2016. Wang et al. (2019) reported based on the 10-years data set that the decadal mean ABLH over Warsaw in summer was of 1.34±0.15 km. This indicates that in terms of the ABLH, the analysed data set can be regarded as representative for the long-term analysis. The mean values of α_{ABL}, AOD_{ABL} and LR_{ABL} calculated at the two wavelengths in the transition time are higher in the sunset (WML) and lower for the sunrise (MTL), the latter being similar to NL. The mean $ÅE_{ABL}$ in the given periods was high (1.37-1.61, in Table 2), indicating small-size particles. (Later on, we will show that for the nocturnal period the $ÅE_{ABL}$ values spread between 0.7 and 2.9, and in the sunrise/sunset period they narrow to 0.8-2.2 range).

The frequency distribution plots for the AOD_{ABL}, LR_{ABL}, $ÅE_{ABL}$ derived at 355 and 532 nm and the FCMR derived for $PM_{2.5}$ and PM_{10} for the entire, nocturnal and sunrise/sunset times are shown in Figure 2. The mean AOD_{ABL} mainly ranges from 0.1-0.3, whereby above 80% of occurrence is attributed to AOD_{ABL} (355) in the range of 0.1-0.3 and AOD_{ABL} (532) of below 0.2. The values of mean LR_{ABL} (355) and LR_{ABL} (532) mainly distribute from 30 to 70 sr, which accounts for more than 75% of total data. The majority of the $ÅE_{ABL}$ (355/532) values are between 1.0 and 2.0 (more than 90% of total data), which indicates mid- and small-size particles ($\leq$ 500 nm) within the boundary layer. On the other hand, the FCMR values between 0.5 and 1.5 constitute around 70% of total data, indicating a more-less equal distribution to fine and coarse particles with a size between 2.5 and 10 μm at the surface. The most of the AOD_{ABL} in MTL is below 0.2 and the LR_{ABL} in MTL ranges from 25 to 50 sr at both wavelengths.

The δ_{ABL} in MTL between 0.04-0.06 accounts for around 50 % of occurrence. The fine particles are expected in MTL due to the majority of FCMR being above 1.5.

Amiridis et al. 2005, reported the 4-years mean AOD_{ABL} of 0.44±0.16 at 355 nm, and the mean LR_{ABL} of 49±25 at 355 nm in summer at Thessaloniki, Greece. According to Papayannis et al. (2008), this much higher value of AOD_{ABL} (355) can be attributed to a significantly stronger impact of the summertime Saharan dust events on Thessaloniki than on Warsaw. Sicard et al. (2011), reported low AOD_{ABL} of 0.07±0.02 at 532 nm in North-eastern Spain, and explained it by the influence of sea-breeze on Barcelona area. Mattis et al. (2004). reported for Leipzig the 3-years mean AOD_{ABL} (355) of 0.38 and AOD_{ABL} (532) of 0.18, with the mean LR_{ABL} (355) of 58 sr and LR_{ABL} (532) of 53 sr, and the mean $ÅE_{ABL}$ (355/532) of 1.4. However, the $ÅE_{ABL}$ was of 1.8-2.2 in the upper boundary layer during summer in Leipzig (Matthias et al., 2004), i.e. during summer only slightly larger particles are observed in ABL in Warsaw as compared to Leipzig. Matthias et al. (2004), derived for Raman lidar observations at 10 EARLINET stations: the lowest AOD_{ABL} values in the northwestern (Aberystwyth) and the highest values in the southeastern Europe (Athens), which was again attributed to the impact of Saharan dust events on the aerosol distribution in Southern Europe.

Lidar ratio was used for the aerosol type characterization in various aerosol typing algorithms (e.g. Papagiannopoulos et al., 2018; Nicolae et al., 2018). Alados-Arboledas et al. (2011), reported lidar ratios of fresh biomass-burning pollution plume of 60–65 sr at 355 nm and 532 nm at Granada. Müller et al., (2007), reported the lidar ratios of 45-60 sr with a mean value of 53 sr at 532 nm, and the particle depolarization ratio at 532 nm below 0.05 for Leipzig, under local and regional urban and anthropogenic haze conditions. Amiridis et al. (2005) reported for Thessaloniki, the continental aerosol 4-year mean lidar ratio of 40-47 sr at 355 nm, and Giannakaki et al. (2010) for the biomass burning aerosol 7-year mean lidar ratio of 70 sr at 355 nm. Optical properties of eight aerosol types were derived by Burton et al. (2012) over North America for the urban aerosol (lidar ratio at 532 nm of 53-70 sr with particle depolarization ratio of 0.03-0.07) and for the smoke particles (lidar ratio of 33-46 sr with particle depolarization ratio of 0.04-0.09). The lidar ratio of marine particles of 20-26 sr at 532 nm was found in North Atlantic and Tropical Indian Ocean by Müller et al. (2007), and 25±4 sr at 532 nm in Hawaii by Masonis et al. (2003). Dawson et al. (2015) presented the global mean lidar ratio for marine aerosol to be 26 sr, with a range from 22±7 to 32±17 sr, depending on variation of mean ocean surface wind speed. Haarig et al. (2017), reported for the marine particles the lidar ratios varying from 19-27 at 355 nm and 23-25 at 532 nm, and particle depolarization ratio of 0.05-0.12 at 355 and 0.07-0.15 at 532 nm. A review of aerosol types reported by Groß et al. (2013; 2015), include in the classification scheme values based on which: the lidar ratio for the marine particles varied from 16-30 sr at 355 nm and 18-26 sr at 532 nm, for the biomass burning 50-95 sr at 355 nm and 60-90 sr at 532 nm, for the mineral dust 50-70 sr at 355 nm and 45-65 sr at 532 nm, for the pollution 50-65 sr at 355 nm and 50-60 sr at 532 nm. In the current study, for several cases LR_{ABL} in the range of 25-30 sr at both wavelengths was obtained (Figure. 2), which is interpreted as likely due to transport of the clean air-mass of Arctic marine particles injected into the boundary layer in Warsaw during the analysed period. Such cold air-masses can be transported from Arctic to Eastern Europe (Costa-Surós et al., 2015).

Linear particle depolarization ratio was an indicator of non-spherical particles (Ansmann et al., 2009; Sakai et al., 2010; Gasteiger and Freudenthaler, 2014). The total depolarization ratio in dust episodes are reported above 0.2, while anthropogenic pollution aerosol have a total depolarization ratio below 0.1 (Xie et al., 2008; Nemuc et al., 2013). Heese and Wiegner (2008), reported

particle depolarization ratio for dust (~ 0.25) and biomass burning aerosol (< 0.1) over Sahel (West Africa). The particle depolarization ratios of dust particles in the range of 0.1-0.25 were reported in Leipzig (Matthias et al., 2004) and 0.3-0.35 at Ouarzazate, Morocco (Freudenthaler et al., 2009). The particle depolarization ratios of urban haze and fire smoke are reported of less than 0.05 at different sites (Müller et al., 2007). The linear particle depolarization ratio for marine aerosol, in the range from 0.01 to 0.03, was reported by Groβ et al. (2011). In the current study, the results of the obtained δ_{ABL} (shown in Figure. 2) are within the range of the listed above values characterizing different aerosol types. As δ is sensitive to the size of the sensed non-spherical particles, in particular small-size particles (< 300 nm) sensed with twice larger wavelength (532 nm) can be under detection limit, as seen in Figure. 2. The dust cases detected in the free troposphere during the given measurement period in Warsaw (e.g. Janicka et al., 2017) were excluded from the current analyses (4 cases), yet the derived δ values of entire observation time are of less than 0.1, which means that there were no cases of dust particles deposited nor advected into the ABL, although polluted dust existence cannot be entirely excluded.

Overall, during period of July to September of 2013, 2015 and 2016 in Warsaw, the aerosol within the ABL consisted mainly of following: i) urban anthropogenic pollution of local origin or transported from areas below or above of the Czech Republic via Silesia and/or Germany (61%), with its mixtures with ii) grass and peatland biomass burning aerosol transported from Russia, Ukraine and Belarus (14%), iii) pollen emissions of strictly local origin form the semi-natural Warsaw's green parks (7%), iv) arctic marine particles transported mainly from Arctic over Baltic Sea (5%). For remaining cases, identification of aerosol composition was regarded as due to a mixture of more than two sub-components (13%), and therefore it was not interpreted. The given percentages were derived as related to the number of profiles with estimated origin to the total number of profiles, and therefore are given without uncertainties. No significant contribution of mineral dust into the boundary layer was found for the 246 analysed profiles, although transport pathways from Sahara over Iberian Peninsula or via Italy were identified for the upper troposphere.

For the collocated simultaneously Raman lidar measurements and the shadowband radiometer measurements, we assessed the AOD_{ABL} contribution within the boundary layer into the AOD_{CL} within the column of air, this having in mind that such collocated measurements never sample the identical air section (lidar sampling in zenith-position versus radiometer sampling at angles related to Sun's elevation over the horizon). So as to make sure that the columnar measurements with less used in the lidar community shadowband radiometer do provide high quality data products, an intercomparison of the MFR-7 shadowband radiometer (PolandAOD-NET, Level 1.5 data, 415 nm and 500 nm) and CE318 sunphotometer (AERONET, Version 3, Level 2.0 data, 380 nm and 500 nm) was performed. The use of the specified above level of data for both networks is defined as a clear sky, manually cloud screened, calibrated within 12 months data products. One month of collocated daytime (03-19 UTC) measurements in July 2018 at RS-Lab in Warsaw was chosen for the intercomparison and confirmed the high quality of measurements performed using both instruments. Figure 3 shows high correlation coefficients (R=0.98) and low standard deviations (STD=0.02) for 144 data points obtained at 380 nm and 500 nm for the intercomparison of the CE318 and MFR-7. Note that in Figure 3, the AOD_{CL} value at 415 nm of MFR-7 was scaled to the value at 380 nm (corresponding to CE318 wavelength) by using Ångström law.

Figure 4 shows the daytime mean 30-60 min average of the aerosol optical depth within the atmospheric boundary layer AOD_{ABL} at 355 and 532 nm, calculated from the mean extinction coefficient profiles of the EARLINET PollyXT lidar in Warsaw and the columnar daytime mean 1h average (with threshold of at least 5 data points) of the AOD_{CL} at 415 and 500 nm (scaled to lidar wavelengths) derived from the PolandAOD-NET MFR-7 shadowband radiometer measurements in Warsaw. Note that, AOD_{CL} of

5   CE318 in Belsk were in good agreement with Warsaw results, with Belsk values being slightly lower than those in Warsaw (compare values in Table 3). Figure 4 depicts also the extinction-derived $ÅE_{ABL}$ (355/532) of lidar and the $ÅE_{CL}$ (355/532) computed from the (scaled) shadowband radiometer AOD_{CL}. Products presented in Figure 4 were derived for period of July-September of 2013, 2015 and 2016, for a subsample of cases when all three instruments were conducting observations at the same time (i.e. 41 cases).

10   In Table 3, the CE318 derived mean AOD is of 0.41±0.17 at 355 nm and 0.23±0.09 at 532 nm, the MFR-7 derived mean AOD is of 0.45±0.17 at 355 and 0.25±0.11 at 532 nm, and the PollyXT derived mean AOD_{ABL} is of 0.20±0.06 at 355 and 0.13±0.03 at 532 nm, for the 41 points. The columnar AOD_{CL} values of the two instruments are the same in the given uncertainty range, despite the distance of 43.7 km between the two sites in Warsaw and Belsk. It can be expected that $AOD_{ABL} < AOD_{CL}$ (e.g. Sicard et al., 2011; Szczepanik and Markowicz, 2018). The obtained results indicate the mean values of the AOD_{ABL} being twice lower than the

15   mean values of AOD_{CL}. High contribution of the aerosol load in the free troposphere can be related to the summertime long range transport of the biomass burning aerosol to Warsaw (e.g. Markowicz et al. 2016; Szkop and Pietruczuk, 2017; Janicka et al., 2017; Stachlewska et al., 2017a; 2018). This is why, in Table.3 in brackets, also the mean values derived for the cases of no long range transport in the free troposphere are listed (i.e. no allocation to categories of forest-fire, dust, etc. in the EARLINET/ACTRIS Data Base). Excluding those cases from the mean, results in the lower AOD_{CL} of roughly 30 to 40 % in Warsaw and ~30 % in Belsk. At

20   the same time, the mean values of AOD_{ABL} do not decrease as much, i.e. AOD_{ABL} is lower of less than 20%. Szczepanik and Markowicz, (2018) proposed for conditions with no aerosol layers in the free troposphere, an approximation of daytime boundary layer aerosol load for the rural mountainous site (Strzyzow, Poland, elevation 899 m a.s.l.) as being of AOD_{ABL} (500) ≈ 80% AOD_{CL} (500). Based on the values listed in the Table 3, such approximation for the urban continental site in Warsaw (elevation 112 m a.s.l.) would be of AOD_{ABL} (532) ≈ 53% AOD_{CL} (532) and AOD_{ABL} (355) ≈ 67% AOD_{CL} (355).

25   In a closer look on Figure 4, the lidar derived AOD_{ABL} are of less than 0.2 on a few days, (e.g. case number 9-13), although corresponding values of radiometer derived AOD_{CL} are more than 0.7. This is not a mistake. On 10 July 2013, the biomass burning aerosol from Canadian wildfires was detected by lidar in Warsaw, with an apparent optically thick aerosol layer suspended in the lower troposphere just above the boundary layer top height, as reported by Janicka et al. (2017) and Ortiz-Amezcua et al. (2017). Due to the low ABLH (< 1000 m) on this day, (not unusual under high pressure system over Poland e.g.

30   Stachlewska et al. (2018), the optical depth contribution of aerosol smoke layer in the free troposphere dominated over the optical depth contribution of the aerosol within the boundary layer, which explains much higher columnar than boundary layer AOD. Markowicz et al. (2016), reported aerosol layers in the free troposphere with significant (up to 55%) contribution to the total optical depth, which is consistent with results obtained in the current paper.

The results in Figure.4 obtained for the ÅE as being related to the particle size, show that retrievals by different instruments have similar trend of variation with time. The mean $ÅE_{CL}$ values given in Table 3, are the same, in the given variability range for all 41 cases, despite the differences in the measurement wavelengths. The values in brackets (no long range transport of aerosol in free troposphere), show consistent results, i.e. the higher $ÅE_{ABL}$ than $ÅE_{CL}$ were obtained, which indicates pollution dominating within the boundary layer.

4.1 Relation of ABLH with optical properties and surface PM in summer and early autumn over Warsaw

The comparison of the AOD_{CL} and AOD_{ABL} with the ABLH for 41 cases of the collocated in time measurements conducted with the MFR-7 and the PollyXT, show the positive correlation (0.74 at both wavelengths) of AOD_{ABL} and ABLH, being even higher than the correlation coefficient of 0.55 between AOD_{ABL} and ABLH reported for Leipzig by Mattis et al. (2004). Similar was reported for Warsaw by Stachlewska et al. (2017b; 2018), i.e. when there is no aerosol in the free troposphere above Warsaw, however therein both AOD_{CL} and AOD_{ABL} were reported to increase with increasing ABLH. In the current study, no significantly correlation was observed for the AOD_{CL} and ABLH, which is related to differences in load and type of aerosol in the free troposphere and within the boundary layer. When aerosol layer containing particles of dust, smoke, pollution or their mixtures is suspended in the free troposphere, an increase of columnar AOD_{CL} values can be observed. Marinou et al. (2017), reported that dust particles can be transported far away from their source of origin and are frequently observed over central and northern Europe, with higher occurrences during summer. Dust particles can occur over Warsaw, mainly in the free troposphere (at the height > 2-3 km) in spring and summer period (Chilinski et al., 2016; Janicka et al., 2017; Szczepanik et al., 2019). Biomass burning particles and smoke layers were detected over central Europe in summers of 2013 (Janicka et al., 2017; Ortiz-Amezcua et al., 2017; Trickl et al., 2015), 2015 (Stachlewska et al., 2017b; Szkop and Pietruczuk, 2017), and 2016 (Stachlewska et al., 2018). The biomass burning and dust were detected and analysed in southern Europe over 10 years lidar dataset (Siomos et al. 2017, 2018). The Canadian wildfire smoke detected in the troposphere and the stratosphere in summer 2017 over central Europe was reported by Haarig et al. (2018), Ansmann et al. (2018), Hu et al. (2019), and Baars et al. (2019).

In the case of lack of clouds (as in this study), the less sufficient growth of the ABLH, could be explained as partly due to the aerosol suspended in the free troposphere, reducing the solar radiation reaching the surface, and thus suppressing the thermal turbulence, and leading to lower boundary layer height. Hence, for certain conditions the relation of AOD_{CL} and ABLH can be expected to exhibit negative correlation.

The majority of the analysed 41 cases of daytime, clear-sky, summertime measurements were related to observations of the biomass burning aerosol in the free troposphere. Over an urban site, the AOD_{ABL} can increase due to pollution in the boundary layer, which adds to the ABLH grow due to the Sun-driven turbulence. At the same time the AOD_{CL} can decrease when the free troposphere aerosol (e.g. absorbing particles) can cause negative radiative effects at the surface. One more aspect have to be accounted additionally for; the presence of aerosol particles in the troposphere directly above the boundary layer top, may follow from the dynamics of turbulent eddy structures in the layer. Even in the absence of convection, a typical feature of turbulent

boundary layer flows is the presence of abrupt bursting and sweeping events (Pope, 2000). Bursts can eject the aerosol particles to the upper regions of the boundary layer. The interactions between vortical structures are responsible for the balances of particle concentration in the boundary layer flows (Béghein et al., 2014).

The AOD_{ABL} is calculated as an integral of the extinction coefficient within ABLH and ABLH is a variable of AOD_{ABL}, therefore ABLH is not expected to be strongly related with the aerosol conditions above in the free troposphere. Aerosol optical depth is unique parameter to determine the atmospheric aerosol load and the ABLH derived by lidar is relying on a higher aerosol concentration within the boundary layer than in the free troposphere. Therefore, a positive correlation of AOD_{ABL} with ABLH can be expected. Note, that although an intrusion of biomass burning smoke into the boundary layer can contribute strongly to suppression of the growth of ABLH, as reported by Stachlewska et al. (2018), it still did not result in a negative correlation.

The relations of lidar derived AOD_{ABL}, $ÅE_{ABL}$ and ABLH at different time period of the day for the July-September of 2013, 2015 and 2016 (246 cases) are depicted in Figure 5. Since the AOD_{ABL} is related to the ABLH, then there is more aerosol load within the ABL, as compared to the free troposphere, and thus a positive correlation can be observed. A relatively high correlation coefficient (0.76 at 355 nm, 0.75 at 532 nm) between ABLH and AOD_{ABL} occurred in MTL, while their correlation coefficients are slightly weaker (0.66 and 0.61, respectively) during the nocturnal time (residual layer effect), when aerosol load within ABL basically remain stable, due to much weaker vertical mixing at night.

The mean $ÅE_{ABL}$ is 1.54±0.37, indicating the domination of relatively small particles in the observation period. No obvious relation between $ÅE_{ABL}$ and ABLH is obtained, but the highest values ($ÅE_{ABL} > 2$) were observed only at night, i.e. either more pollution or less humidity. Indeed, a higher concentration of $PM_{2.5}$ was measured during the nocturnal time (16.75±6.86 µg/m^3), as compared to the other periods (15.74±7.24 µg/m^3 in the sunrise and 10.94±4.13 µg/m^3 in the sunset time). Note that given standard deviations indicate high variability of the obtained values.

Figure 6 illustrates the relations between the ABLH, $PM_{2.5}$, PM_{10}, and FCMR. Some negative trend for the well-mixed layer between FCMR with ABLH can be observed, which may suggest an increase of coarse particles (number or/and size) at the surface with an ascending ABLH. It cannot be excluded that, adiabatic effects have partly influenced the growth of particle size. Schäfer et al. (2006), found a high negative correlation between PM_{10} and ABLH in Hanover and Munich in winter. Rost et al. (2009), reported a strong negative relation between PM_{10} and ABLH in Stuttgart. Similarly, Du et al. (2013), find that $PM_{2.5}$ and ABLH exhibit negative correlation in Delhi and Xi'an. Geiß et al. (2017), reported that the link between the PM and ABLH can be attributed to several different reasons, such as meteorological conditions, terrain, local particle sources and even to the method of the ABLH retrieval itself. This was also the case for Warsaw during long-range transported aerosol injections into the boundary layer (Stachlewska et al., 2017b; 2018). However, in general, no pronounced relationship between the PM_{10} and ABLH are expected for Warsaw, as in Zawadzka et al. (2013). Also in the current study, no significant link between particulate matter (PM_{10} and $PM_{2.5}$) and ABLH was found for Warsaw during summer and early-autumn (Figure 6), which at least partly can attributed to relatively low records of PM_{10} emissions (hourly values < 60 µg/m^3) and relatively high summer ABLHs (up to 1.6 km, Table 2). The highest PM_{10} and $PM_{2.5}$ are observed at night (NL and RL), lower for MTL, and the lowest for WML. Reizer and Juda-Rezler (2015), reported that either regional background pollution or local emission sources are mainly responsible for the high PM_{10} and

PM$_{2.5}$ concentrations in Polish urban areas. Clearly, the ABLH is not the main factor controlling the surface pollution in summer in Warsaw, which is consistent with the reports by Bonn et al. (2016), Stachlewska et al. (2017b; 2018), and Geiß et al. (2017).

4.2 Interrelations within optical properties and with surface PM in summer and early autumn over Warsaw

Figure 7 presents the relationship of AOD$_{ABL}$, ÅE$_{ABL}$, LR$_{ABL}$, δ$_{ABL}$ and surface FCMR for the nocturnal and transition times during July, August and September in 2013, 2015 and 2016. The separation thresholds for FCMR are defined as follows: FCMR > 1.5 (vertical line) means that fine particles (< 2.5 µm) dominated and FCMR < 0.5 (vertical dashed line) means domination of coarse particles (2.5-10 µm). The given thresholds for ÅE roughly indicate dominating particle size distribution mode, with separation thresholds of for small particles ÅE > 1.5 (horizontal line) and large particles ÅE < 1 (horizontal dashed line). However, relation between ÅE and aerosol size distribution is complicated, and so it is for the FCMR.

For all time periods, the values of FCMR between 0.5 and 1.5 constitute the largest proportion in total. In the nocturnal time there is more fine particles than at sunrise (MTL), than at sunset (WML). There is clear separation mark at FCMR of 1.5, regardless the time period and no clear correlation of ÅE$_{ABL}$ and FCMR, however for 1 < ÅE$_{ABL}$ < 2 at the nocturnal time and at sunrise, there is higher PM$_{2.5}$ contribution at the surface.

Because of a weak vertical air motion (no convective mixing) and lower ABLH during the nighttime, relatively large aerosol particles are deposited in ABL, and most of small aerosol particles stack below the inversion of boundary layer top (or residual layer). This can lead to an increase of number of small particles accumulated within nocturnal ABL, which manifest as fine particles increase at surface. In general, urban pollution, regarded as road traffic, industrial emission and chemical reaction of gases (SO$_2$, NO$_2$, NO$_x$), causes increase of both PM$_{10}$ and PM$_{2.5}$ (He et al., 2008). The sunrise time in July-September (05:00-09:00 local time) corresponds to urban traffic emission, which can cause lifting of particles from the ground (Zawadzka et al., 2013). The relationship of LR$_{ABL}$ and FCMR in Figure 7 shows clear separation of data, being mainly a result of higher abundance of the fine particles in MTL. On the contrary, more coarse particles (PM$_{10}$ with higher LR$_{ABL}$ of 40-80 sr) occur in WML.

The relationship of δ$_{ABL}$ and FCMR in Figure 7 indicates possible negative trends (stronger at 532 nm) for all time periods. The abundance of the fine (coarse) particles at the surface is related to the abundance of the spherical particles within the ABL.

Bennouna et al. (2016), reported that a significant positive correlation of PM$_{10}$ and AOD$_{CL}$, and increasing correlation coefficient for daily, monthly and yearly averages, relays on the aerosol characteristics of the site. Zawadzka et al. (2013), reported a negative correlation between PM$_{10}$ and AOD$_{CL}$ for long-term monthly mean values in winter in Belsk and Warsaw, and a positive relation for unstable (meaning strong turbulent vertical mixing in summer) atmospheric condition in Warsaw. Relation between optical properties and surface aerosol mass concentration depends on boundary layer processes, chemical composition, source regions, weather conditions and aerosol type, which is challenging to be well characterized by the columnar AOD$_{ABL}$ and the surface PM concentrations alone. Depicted in Figure 7, AOD$_{ABL}$ and FCMR indicates higher AOD$_{ABL}$ for coarse particles (PM$_{10}$) in WML and lower for fine particles (PM$_{2.5}$) in MTL, however, no significant correlations of AOD$_{ABL}$ with PM$_{10}$ or PM$_{2.5}$ are reported in the current study.

The significant correlations (R> 0.5) of AOD_{CL} and $PM_{2.5}$ were reported mainly for eastern cities of China (Guo et al., 2009; Zheng et al., 2015; Zang et al., 2017) and United State (Liu et al., 2007; Hutchison et al., 2008; Wang and Christopher, 2003), where the main industrial regions with extreme pollution are located. In those cases, the majority of aerosol was expected to be present within the boundary layer. The anthropogenic pollution in Warsaw is much lower if compared to the above mentioned regions, Zawadzka et al. (2013), reported R of 0.42 between AOD_{CL} and $PM_{2.5}$ in Warsaw, which was explained as due to a significant load in the free troposphere affecting this relation. The current study shows that also for AOD_{ABL} and $PM_{2.5}$ there is no significant correlation, which can be explained by the low values of AOD_{ABL} and $PM_{2.5}$ measured during the investigated period, so as due to the lack of high pollution events in summer and early autumn in Warsaw. Stachlewska et al. (2017b; 2018) showed that AOD_{ABL} and $PM_{2.5}$ in Warsaw can be correlated, under a high aerosol load conditions during events of an injection of the long-range transported pollution or biomass burning into the boundary layers (but with no aerosol in the free troposphere).

As for the relation of AOD_{ABL} and PM_{10}, in the current study, there was no significant linear correlation of for the nocturnal time found (similar to Filip and Stefan, 2011) and a weak positive relation was observed for the sunrise/sunset time (similar to Zawadzka et al. 2013). The ABL in summer is primarily driven by intensive convective mixing; resulting in significantly higher ABLH than in other seasons (Wang et al., 2019). In summer, the ABL aerosol can be elevated by effective convection to the free troposphere, and this can lead to decrease of aerosol loading within ABL, as reported by e.g. He et al. (2008) and Tian et al. (2017). The emission of PM_{10} in summer is lower than for the other seasons in Warsaw (Zawadzka et al., 2013). Even less urban emissions at night reduce the mass concentrations of surface PM_{10}, and at the same time, the aerosol properties within ABL are relatively stable due to the stable boundary layer in nighttime. Therefore, no apparent relationship can be observed in the nocturnal time.

Interrelations of optical properties within ABL are given in Figure 8. A positive correlation of AOD_{ABL} and LR_{ABL} is observed for all times, being higher for sunrise and sunset (0.64-0.72) and lower for the nocturnal time (~ 0.56). The AOD_{ABL} and LR_{ABL} depend on extinction coefficient derived within the ABL, thus both values will increase when the fine particle contribution increases and/or when there is an increase of the absorption capability of the particles within the ABL, and vice versa. This may be partly due to the presence of biomass burning particles inside the ABL, as e.g. in Stachlewska et al. (2018).

The relation between $ÅE_{ABL}$ and LR_{ABL} shows weak negative trend during the analysed period, which may be due to the larger size particles being injected into the ABL, the particles growing in the ABL or the smoke contribution in composition of the ABL aerosol. As for the latter, the presence of the smoke particles results in a high negative correlations, e.g. correlations between LR_{ABL} and $ÅE_{ABL}$ of -0.79 (Giannakaki et al., 2010) and -0.84 (Amiridis et al., 2009) were found for smoke particles. Also Stachlewska et al. (2018) showed negative correlation of $ÅE_{ABL}$ and LR_{ABL} for smoke particles. Alternative explanation could be as due to the condensation of large organic molecules and particle coagulation from the upper atmosphere into the ABL, as reported by e.g. Pósfai et al. (2004) and Fiebig et al (2003). Giannakaki et al. (2010), showed no significant correlation of $ÅE_{ABL}$ and LR_{ABL} for continental and urban aerosol related with anthropogenic pollution. Also Mattis et al. (2004) reported no relationship between $ÅE_{ABL}$ and LR_{ABL} when anthropogenic particles dominated in Leipzig. The obtained in current paper results suggest that during summer and early autumn in Warsaw, a mixture of a local urban anthropogenic aerosol with a natural source

aerosol (local or long-range transported into ABL), might be a reasonable explanation for observing the weak negative tendency of ÅE_{ABL} and LR_{ABL}.

4.3 Relations of optical properties, surface PM and relative humidity in summer and early autumn over Warsaw

Relations between the near-surface relative humidity (RH) with surface PM_{10} and $PM_{2.5}$ and FCMR and with the lidar derived aerosol properties (AOD_{ABL} $\text{ÅE}_{ABL,}$ LR_{ABL} and δ_{ABL}) were searched for the entire, nocturnal and sunrise/sunset times were investigated. Additionally, the nighttime relation between the lidar derived water vapour mixing ratios (WV_{ABL}) and the aforementioned quantities were investigated.

Generally, in Figure 9, a weak positive trend of RH and $PM_{2.5}$ is in agreement with the results of Sharma et al. (2017). The RH and FCMR exhibit positive correlation, with correlation coefficients of 0.6 for NT, 0.63 for WML and 0.71 for MTL. Zhang et al. 2015 reported that the high RH can led to the high $PM_{2.5}$ in Beijing. Li et al. (2017), showed that in the summer urban environment, due to the hygroscopic effect on aerosol, an increase of the relative humidity can lead to a growth of the fine particles $PM_{2.5}$, but not to a growth of PM_{10}, mainly attributed to the effects of the wet scavenging under the high summer rainfall. The mean relative humidity obtained in the current study was the highest for MTL (63 ± 10 %), then for NL (57 ± 12 %), and the lowest for WML (43 ± 10 %). The small particles have greater possibility to aggregate into relatively large particles at nighttime, and thus the lower correlation coefficients for RH and $PM_{2.5}$ (and FCMR) are found for the nocturnal time.

Figure 10 presents no clear relation of WV_{ABL} with surface $PM_{2.5}$, PM_{10} and FCMR at nighttime in Warsaw. The correlation coefficient of WV_{ABL} and $PM_{2.5}$ is a little higher than WV_{ABL} and PM_{10}, indicating that at night the water vapour in ABL can affect the surface fine particles more than the surface coarse particles. This could be due to the presence of anthropogenic particles in the ABL, as these hygroscopic particles can absorb water vapour and gradually increase in size, although the growth of particles due to coagulation of particles within ABL cannot be excluded (Fiebig et al., 2003).

Figure 10 depicts also no clear relations between WV_{ABL} and AOD_{ABL}, ÅE_{ABL} and LR_{ABL}; only δ_{ABL} and WV_{ABL} show a negative trend. The hygroscopicity of particles increases with decreasing particle size, Petters et al. 2009. At the same time, the more fine particles the lower the depolarization (see Figure 7). Hence, increase of water vapour and presence of hygroscopic particles leads to decrease of depolarization. For the occurrence of a long range transported biomass burning aerosol over Warsaw, hygroscopic effects can be well captured with quasi-continuous profiling of the water vapour (Stachlewska et al., 2017a). Note that the relation of the AOD_{ABL}, ÅE_{ABL} and LR_{ABL} with the surface RH also shows not much of a trend for NL, however for WML the negative trends and properties grouping becomes more visible (Figure 11).

The AOD_{CL} was reported to increase with an increase of the ambient relative humidity for the hygroscopic particles due to the hygroscopic growth (Bergin et al., 2000; Altaratz et al., 2013). In Figure 11, a negative relation between AOD_{ABL} and surface RH is found (with higher surface RH, lower AOD_{ABL} is observed), except for nocturnal time (no trend in Figure 11, similar as in Figure 10 for AOD_{ABL} and WV_{ABL}). The size and optical properties can change as aerosol particles uptake water and higher RH is more favourable for hygroscopic growth of pollution particles (Tang, 1996). During observational period, within the boundary

layer the urban anthropogenic aerosol was observed most frequently. An increase of RH leads to increasing pollution particle size, which is visible at nighttime (ÅE and RH show slight negative trend). A slight positive trend between ÅE_{ABL} and RH is at transition times (different grouping in moister MTL and drier WML), which is being in accordance with the FCMR and ÅE scatter plots (more coarse particles in MTL and more fine particles in WML). Pollution particles within boundary layer due to a

5   weaker convective mixing at nighttime, are prone to water uptake, which contributes to an increase of aerosol particle size Cheng et al. (2008). The relation between LR_{ABL} and RH shows practically no correlation in the nocturnal time but it is well separated in the transition time (lower LR for MTL). At nighttime, increasing LR due to accumulation of hygroscopic smoke particles was reported by Giannkaki et al. (2010). The convection and the energy exchange is stronger in the transition time (Stull, 1988), leading to domination pf the anthropogenic aerosol in the atmospheric boundary layer. Increasing the surface RH results in the rise

10   of the aerosol particles size, and thus contributes to decreasing of LR_{ABL}. The negative trend in relation between δ_{ABL} and surface RH (nicely pronounced at the nocturnal time) is in agreement with the trend obtained for WV_{ABL} and δ_{ABL}.

5 Conclusions

This study comprises the optical properties derived within the atmospheric boundary layer, based on the dataset of July-September of 2013, 2015 and 2016 the EARLINET/ACTRIS site in Warsaw. Interrelations of the different optical properties within ABL as

15   well as relations between them and the surface PM concentrations and RH measurements were studied by conducting comparisons of various parameters in different periods: the entire time (24h, ABL), nighttime (21:00-02:00 UTC; NL and RL), sunrise (03:00-08:00 UTC; MTL) and sunset (16:00-20:00 UTC; WML).

At both wavelengths, AOD_{ABL} and LR_{ABL} at sunset were found to be higher (0.14-0.24 for AOD_{ABL} and 49-55 sr for LR_{ABL}) than for the other two periods (0.06-0.18 for AOD_{ABL} and 32-47 sr for LR_{ABL}). In nocturnal period, ÅE_{ABL} values are higher (1.58±0.36

20   for NL, 1.61±0.37 for RL) than for the two remaining periods (1.53±0.30 for MTL, 1.37±0.34 for WML). Within the entire dataset, the AE_{ABL} was distributed between 1 and 2 (> 90% of data points) and the surface FCMR between 0.5 and 1.5 (~70% of data points). Aerosol composition within ABL of summer and early autumn in Warsaw consisted of urban anthropogenic pollution and its mixtures with local pollen and long range transported biomass burning aerosol and arctic marine particles.

The boundary layer AOD_{ABL} contribution to columnar AOD_{CL} was assessed. The latter was more than twice higher when optically

25   thick aerosol layers were observed above the ABL, and less than twice higher for cases with no aerosol layers in the free troposphere but with presence of aloft pollution due to convection.

The AOD_{ABL} and ABLH exhibit positive correlation (~ 0.75) in the analysed observation period, highest for WML and MTL. When ABLH grows, a declining trend of FCMR is observed for WML, indicating an increase of coarse particle fraction. However, there is no clearly apparent link between PM_{10} or $\text{PM}_{2.5}$ and ABLH. For MTL, the ranges of obtained values of ÅE_{ABL}

30   and FCMR are higher than for WML. A negative correlation of δ_{ABL} and FCMR was found for all time-periods, which indicates higher sphericity of fine particles. Reported in literature, different correlations obtained for AOD_{ABL} and PM_{10} are explained as due to complicated atmospheric and weather conditions. In summer and early autumn in Warsaw, generally high-pressure systems

govern the dynamics of the atmosphere, there is significantly less traffic pollution (people on holidays, on bicycles), and pollination of plants plays a role.

The relation between AOD_{ABL} and FCMR reported here, displays a negative correlation at sunrise and sunset, which can be related to the traffic peaks. Due to less urban emissions (neither traffic nor domestic heating in summer) and stable boundary layer, no

5 apparent relationship of AOD_{ABL} with FCMR was observed at night. The AOD_{ABL} and LR_{ABL} depend on the extinction coefficient within ABL, thus their positive correlation is observed. Relation of $ÅE_{ABL}$ and LR_{ABL} reveals weak negative trend. The positive trends of RH and FCMR were found at night and for sunrise and sunset, whereby the sunrise trend was most pronounced.

The weak positive relation at night for WV_{ABL} and $PM_{2.5}$ is higher than with PM_{10}, indicating that water vapour in NL and RL affects surface fine particles more than surface coarse particles. The increasing WV_{ABL} (and RH at surface) can lead to a decrease

10 of depolarization (both relations are very similar at night) in the presence of the hygroscopic particles. For high near-surface RH lower AOD_{ABL} were derived in MTL and WML, which was not seen in NL and RL. A negative trend of δ_{ABL} and WV_{ABL}, δ_{ABL} and RH is due to the hygroscopicity of particles. A negative relation between AOD_{ABL} and surface RH is found for transition time (both MTL and WML), which is followed by a weak negative correlation of LR_{ABL} and RH observed only during sunset time (WML).

15 The collocated measurements conducted in Warsaw with the MFR-7 shadowband radiometer (PolandAOD-NET) and the CE318 sunphotometer (AERONET) showed a high agreement with the correlation coefficient R of 0.98 and the standard deviation of 0.02 at both 380 nm and 500 nm.

The obtained results contribute to increase of knowledge on variability of optical properties within summer and early autumn atmospheric boundary layer at a continental urban site in central Europe. Relations found in already published research, obtained

20 on the basis of case-study approach, do not necessarily apply nor are seen in the long-term study. Therefore, special care should be taken when interpreting and comparing the different results.

Bottom line is that regular, automated observations of the NeXT generation PollyXT lidar conducted at the EARLINET site in the frame of the ACTRIS infrastructure activities allow for such studies. The excellent capabilities of this lidar enabled combining of the derived within this study results with other data sources (e.g. AERONET, WIOS, PolandAOD). Hypothesis for boundary layer

25 aerosol properties interrelations were proposed and will be further verified with more lidar data of regular observations in Warsaw. What could be improved by enlarging the existing high-quality lidar data sample is an investigation of subgrouping of aerosol properties that could provide statistically significant correlations. Further, more observations will allow for extension of search for differences to other seasons, daytime analyses, and better distinguishing between sunset and sunrise aerosol properties relationships. Finally, a separation of aerosol properties accordingly to aerosol content, i.e. urban aerosol versus its mixture with

30 other aerosol types, would be possible (currently too little data in mixed categories), followed by an estimation of their radiative effect.

Acknowledgments:

This research has been done in the frame of the Technical assistance for Polish Radar and Lidar Mobile Observation System (POLIMOS) funded by ESA-ESTEC Contract No. 4000119961/16/NL/FF/mg.

The PollyXT-Warsaw lidar was developed in a scientific collaboration of the Faculty of Physics, University of Warsaw (FUW) with the Institute of Tropospheric Research (TROPOS). This development was financed by the Polish Foundation of Science and Technology (FNTP-No. 519/FNITP/115/2010). We especially acknowledge colleagues of the PollyXT Lidar Group lead by Dietrich Althausen.

Authors acknowledge the Warsaw Regional Inspectorate of Environmental Protection WIOS-Warsaw for provision of the processed $PM_{2.5}$ and PM_{10} data, visualised at http://www.wios.warszawa.pl. The data were accessed via the Data Archive of the National Chief Inspectorate for Environmental Protection (GIOS) via http://powietrze.gios.gov.pl/pjp/archive.

We acknowledge Brent Holben for processing of the AERONET data (https://AERONETl .gsfc.nasa.gov); Aleksander Pietruczuk and Piotr Sobolewski of Institute of Geophysics at Polish Academy of Sciences for performing the AERONET measurements in Belsk; Phillippe Golub for performing instrument calibrations at the PHOTONS/AERONET-EUROPE calibration center, supported by ACTRIS-1 project funded within the European Union Seventh Framework Program (FP7/2007e2013) under Grant Agreement No.262254. The AERONET sunphotometer at RS-Lab site in Warsaw is a property of the National Institute of Research and Development for Optoelectronics (INOE 2000) in Romania, kindly lend to us by the research group lead by Doina Nicolae, within the frame of the SAtellite based Monitoring Initiative for Regional Air quality (SAMIRA) funded by ESA-ESRIN Contract No. 4000117393/16/INB

We acknowledge Krzysztof Markowicz for processing of the MFR-7 data within the Polish aerosol Research Network PolandAOD-NET (https://polandaod.pl). The MFR-7 radiometer was purchased within a grant No.1283/B/P01/2010/38 of the Polish Ministry of Science and High Education.

The EARLINET activities have been supported by the ACTRIS project funded within the European Commission 7th Framework Programme under Research Infrastructures for Atmospheric Research Grant Agreement No. 262254, the ACTRIS-2 project, funded by the European Union Research Infrastructure Action under the H2020 specific program for Integrating and opening existing national and regional research infrastructures of European interest, Grant Agreement No. 654109 and the ACTRIS PPP project supported by the European Commission under the Horizon 2020 – Research and Innovation Framework Programme, H2020-INFRADEV-2016-2017, Grant Agreement No. 739530. The University of Warsaw participated in the ACTRIS-2 project as an associate partner without funding.

Author Contributions:

I.S.Stachlewska wrote the paper, obtained funding for the research, came up with the study approach, designed methodology, and performed experiment, contributed to development of PollyXT-Warsaw lidar and lidar evaluation algorithms, took care of quality assurance of lidar measurements and data products, and holistically interpreted the lidar results with other data sources results (AERONET, PolandAOD-NET, WIOS Monitoring Network). D.Szczepanik contributed with calculation of the aerosol optical properties profiles (α, β, δ) and with their categorization for the EARLINET/ACTRIS Data Base. D.Wang contributed with extensive literature review, wrote the codes for the ABLH and the WV retrieval algorithms, and performed statistical analysis of the optical properties (AE, LR, δ, WV). All authors contributed with merit revisions of the paper.

Conflicts of Interest:

The authors declare no conflict of interest.

Appendix: Lists of symbols and physical quantities:

Entire time	-- ET
Nocturnal time	-- NT
Transition rime	-- TT
Atmospheric boundary layer (derived by lidar)	-- ABL
Atmospheric boundary layer height (derived by lidar)	-- ABLH
Residual layer (derived by lidar)	-- RL
Nocturnal layer (derived by lidar)	-- NL
Morning transition layer (derived by lidar)	-- MTL
Well-mixed layer (derived by lidar)	-- WML
Particle extinction coefficient (within atmospheric boundary layer)	-- α_{ABL}
Particle backscatter coefficient (within atmospheric boundary layer)	-- β_{ABL}
Aerosol optical depth (within atmospheric boundary layer, derived by lidar)	-- $AOD_{ABL}(\lambda)$
Aerosol optical depth (columnar, derived by sun-photometer or radiometer)	-- $AOD_{CL}(\lambda)$
Lidar ratio (within atmospheric boundary layer)	-- $LR_{ABL}(\lambda)$
linear particle depolarization ratio (within atmospheric boundary layer)	-- $\delta_{ABL}(\lambda)$
Ångström exponent (within atmospheric boundary layer, derived by lidar)	-- $\text{ÅE}_{ABL}(\lambda_1/\lambda_2)$

Ångström exponent (columnar, derived by sun-photometer or radiometer)   -- $\text{ÅE}_{\text{CL}}(\lambda_1/\lambda_2)$

Water vapor mixing ratio (within atmospheric boundary layer)   -- WV_{ABL}

Relative humidity (at the near-surface)   -- RH

Particulate matter with diameter <10 μm; <2.5 μm   -- PM_{10}; $\text{PM}_{2.5}$

Fine to coarse mass ratio   -- FCMR

Wavelength   -- λ

References

Ångström, A.: On the atmospheric transmission of sun radiation and on dust in the air, Geogr. Ann., 12, 156–166, https://doi.org/10.1080/20014422.1929.11880498, 1929.

Altaratz, O., Bar-Or, R. Z., Wollner, U., and Koren, I.: Relative humidity and its effect on aerosol optical depth in the vicinity of convective clouds, Environ. Res. Lett., 8, 034025, https://doi.org/10.1088/1748-9326/8/3/034025, 2013.

Alados-Arboledas, L., Müller, D., Guerrero- Rascado, J., Navas-Guzmán, F., Pérez-Ramírez, D., and Olmo, F.: Optical and microphysical properties of fresh biomass burning aerosol retrieved by Raman lidar, and star- and sun- photometry, Geophys. Res. Lett., 38, https://doi.org/10.1029/2010GL045999, 2011.

Amiridis, V., Balis, D., Kazadzis, S., Bais, A., Giannakaki, E., Papayannis, A., and Zerefos, C.: Four- year aerosol observations with a Raman lidar at Thessaloniki, Greece, in the framework of European Aerosol Research Lidar Network (EARLINET), J. Geophys. Res., 110, https://doi.org/10.1029/2005JD006190, 2005.

Amiridis, V., Balis, D., Giannakaki, E., Stohl, A., Kazadzis, S., Koukouli, M., and Zanis, P.: Optical characteristics of biomass burning aerosol over Southeastern Europe determined from UV-Raman lidar measurements, Atmos. Chem. Phys., 9, 2431-2440, https://doi.org/10.5194/acp-9-2431-2009, 2009.

Ansmann, A., Tesche, M., Knippertz, P., Bierwirth, E., Althausen, D., Mueller, D., and Schulz, O.: Vertical profiling of convective dust plumes in Southern Morocco during SAMUM, Tellus B: Chem. and Phys. Meteo., 61, 340-353, https://doi.org/10.1111/j.1600-0889.2008.00384.x, 2009.

Ansmann, A., Baars, H., Chudnovsky, A., Mattis, I., Veselovskii, I., Haarig, M., Seifert, P., Engelmann, R., and Wandinger, U.: Extreme levels of Canadian wildfire smoke in the stratosphere over Central Europe on 21–22 August 2017, Atmos. Chem. Phys., 18, 11831-11845, https://doi.org/10.5194/acp-18-118312018, 2018.

Baars, H., Kanitz, T., Engelmann, R., Althausen, D., Heese, B., Komppula, M., Preißler, J., Tesche, M., Ansmann, A., Wandinger, U, Lim, J.-H., Ahn, J. Y., Stachlewska, I. S., Amiridis, V., Marinou, E., Seifert, P., Hofer, J., Skupin, A., Schneider, F., Bohlmann, S., Foth, A., Bley, S., Pfüller, A., Giannakaki, E., Lihavainen, H., Viisanen, Y., Hooda, R. K., Pereira, S. N., Bortoli, D., Wagner, F., Mattis, I., Janicka, L., Markowicz, K. M., Achtert, P., Artaxo, P., Pauliquevis, T., Souza, R. A. F., Sharma, V. P., van Zyl, P. G., Beukes, J. P., Sun, J., Rohwer, E. G., Deng, R., Mamouri, R.-E., and Zamorano, F.: An overview of the first decade of Polly[NET]: An emerging network of automated Raman-polarization lidars

for continuous aerosol profiling, Atmos. Chem. Phys., 16, 5111-5137, https://doi.org/10.5194/acp-16-5111-2016, 2016.

Baars, H., Ansmann, A., Ohneiser, K., Haarig, M., Engelmann, R., Althausen, D., Hanssen, I., Gausa, M., Pietruczuk, A., Szkop, A., Stachlewska, I. S., Wang, D., Reichhardt, J., Skupin, A., Mattis, I., Trickl, T., Vogelmann, H., Navas-Guzmán, F., Haefele, A., Acheson, K., Ruth, A. A., Tatarov, B., Müller, D., Hu, Q., Podvin, T., Goloub, P., Vesselovski, I., Pietras, C., Haeffelin, M., Fréville, P., Sicard, M., Comerón, A., Fernández García, A. J., Molero Menéndez, F., Córdoba-Jabonero, C., Guerrero-Rascado, J. L., Alados-Arboledas, L., Bortoli, D., Costa, M. J., Dionisi, D., Liberti, G. L., Wang, X., Sannino, A., Papagiannopoulos, N., Boselli, A., Mona, L., D'Amico, G., Romano, S., Perrone, M. R., Belegante, L., Nicolae, D., Grigorov, I., Gialitaki, A., Amiridis, V., Soupiona, O., Papayannis, A., Mamouri, R.-E., Nisantzi, A., Heese, B., Hofer, J., Schechner, Y. Y., Wandinger, U., and Pappalardo, G.: The unprecedented 2017–2018 stratospheric smoke event: Decay phase and aerosol properties observed with EARLINET, Atmos. Chem. Phys. Discuss., https://doi.org/10.5194/acp-2019-615, in review, 2019.

Barlage, M., Miao, S., and Chen, F.: Impact of physics parameterizations on high-resolution weather prediction over two Chinese megacities, J. Geophys. Res., 121, 4487-4498, https://doi.org/10.1002/2015JD024450, 2016.

Bennouna, Y., Cachorro, V. E., Mateos, D., Burgos, M. A., Toledano, C., Torres, B., and de Frutos, A.: Long-term comparative study of columnar and surface mass concentration aerosol properties in a background environment, Atmos. Environ., 140, 261-272, https://doi.org/10.1016/j.atmosenv.2016.05.061, 2016.

Bergin, M. H., Schwartz, S. E., Halthore, R. N., Ogren, J. A., and Hlavka, D. L.: Comparison of aerosol optical depth inferred surface measurements with that determined by Sun photometry for cloud-free conditions at a continental US site, J. Geophys. Res., 105, 6807–6816, https://doi.org/10.1029/1999JD900454, 2000.

Béghein C., Allery C., Wacławczyk C., and Pozorski J.: Application of POD-based dynamical systems to dispersion and deposition of particles in turbulent channel flow, Int. J. Multiphase Flow, 58, 97-113, https://doi.org/10.1016/j.ijmultiphaseflow.2013.09.001, 2014.

Bonn, B., von Schneidemesser, E., Andrich, D., Quedenau, J., Gerwig, H., Lüdecke, A., Kura, J., Pietsch, A., Ehlers, C., Klemp, D., Kofahl, C., Nothard, R., Kerschbaumer, A., Junkermann, W., Grote, R., Pohl, T., Weber, K., Lode, B., Schönberger, P., Churkina, G., Butler, T. M., and Lawrence, M. G.: BAERLIN2014 – the influence of land surface types on and the horizontal heterogeneity of air pollutant levels in Berlin, Atmos. Chem. Phys., 16, 7785-7811, https://doi.org/10.5194/acp-16-7785-2016, 2016.

Böckmann, C., Wandinger, U., Ansmann, A., Bösenberg, J., Amiridis, V., Boselli, A., Delaval, A., De Tomasi, F., Frioud, M., and Grigorov, I. V.: Aerosol lidar intercomparison in the framework of the EARLINET project. 2. Aerosol backscatter algorithms, Appl. Opt., 43, 977-989, https://doi.org/10.1364/AO.43.000977, 2004.

Böckmann, C., Mironova, I., Müller, D., Schneidenbach, L., Nessler, R.: Microphysical aerosol parameters from multiwavelength lidar, J. Opt. Soc. Am. A, 22(3), 518–528, https://doi.org/10.1364/JOSAA.22.000518, 2005.

Binietoglou, I., Basart, S., Alados-Arboledas, L., Amiridis, V., Argyrouli, A., Baars, H., Baldasano, J. M., Balis, D., Belegante, L., Bravo-Aranda, J. A., Burlizzi, P., Carrasco, V., Chaikovsky, A., Comerón, A., D'Amico, G., Filioglou, M., Granados-Muñoz, M. J., Guerrero-Rascado, J. L., Ilic, L., Kokkalis, P., Maurizi, A., Mona, L., Monti, F., Muñoz-Porcar, C., Nicolae, D.,

Papayannis, A., Pappalardo, G., Pejanovic, G., Pereira, S. N., Perrone, M. R., Pietruczuk, A., Posyniak, M., Rocadenbosch, F., Rodríguez-Gómez, A., Sicard, M., Siomos, N., Szkop, A., Terradellas, E., Tsekeri, A., Vukovic, A., Wandinger, U., and Wagner, J.: A methodology for investigating dust model performance using synergistic EARLINET/AERONET dust concentration retrievals, Atmos. Meas. Tech., 8, 3577-3600, https://doi.org/10.5194/amt-8-3577-2015, 2015.

Burton, S. P., Ferrare, R. A., Hostetler, C. A., Hair, J. W., Rogers, R. R., Obland, M. D., Butler, C. F., Cook, A. L., Harper, D. B., and Froyd, K. D.: Aerosol classification using airborne High Spectral Resolution Lidar measurements–methodology and examples, Atmos. Meas. Tech., 5, 73-98, https://doi.org/10.5194/amt-5-73-2012, 2012.

Burton, S. P., Hair, J. W., Kahnert, M., Ferrare, R. A., Hostetler, C. A., Cook, A. L., Harper, D. B., Berkoff, T. A., Seaman, S. T., Collins, J. E., Fenn, M. A., and Rogers, R. R.: Observations of the spectral dependence of linear particle depolarization ratio of aerosol using NASA Langley airborne High Spectral Resolution Lidar, Atmos. Chem. Phys., 15, 13453-13473, https://doi.org/10.5194/acp-15-13453-2015, 2015.

Cheng, Y. F., Wiedensohler, A., Eichler, H., Heintzenberg, J., Tesche, M., Ansmann, A., Wendisch, M., Su, H., Althausen, D., Herrmann, H., Gnauk, T., Brüggemann, E., Hu, M., and Zhang, Y. H.: Relative humidity dependence of aerosol optical properties and direct radiative forcing in the surface boundary layer at Xinken in Pearl River Delta of China: An observation based numerical study, Atmos. Environ., 42, 6373–6397, https://doi.org/10.1016/j.atmosenv.2008.04.009, 2008.

Chen, B., and Kan, H.: Air pollution and population health: A global challenge, Environ. Health Prev. Med., 13, 94-101, https://doi.org/10.1007/s12199-007-0018-5, 2008.

Chilinski, M. T., Markowicz, K. M., Zawadzka, O., Stachlewska, I. S., Kumala, W., Petelski, T., Makuch, P., Westphal, D. L., and Zagajewski, B.: Modelling and Observation of Mineral Dust Optical Properties over Central Europe, Acta Geophys., 64 (6), 2550-2590, https://doi:10.1515/acgeo-2016-0069, 2016.

Costa-Surós, M., Stachlewska, I. S., Nemuc, A., Talianu, C., Heese, B., and Engelmann, R.: Study case of air-mass modification over Poland and Romania observed by the means of multiwavelength Raman depolarization lidars, the 27th International Laser Radar Conference, New York, USA, 5-10 July 2015, 1-4, 2015.

Comerón, A., Sicard, M., and Rocadenbosch, F.: Wavelet Correlation Transform Method and Gradient Method to Determine Aerosol Layering from Lidar Returns: Some Comments, J. Atmos. Ocean. Tech., 30, 1189–1193, https://doi.org/10.1175/JTECH-D-12-00233.1, 2013.

Dang, R.; Yang, Y.; Hu, X.-M.; Wang, Z.; Zhang, S.: A Review of Techniques for Diagnosing the Atmospheric Boundary Layer Height (ABLH) Using Aerosol Lidar Data, Remote Sens., 11, 1590, https://doi.org/10.3390/rs11131590, 2019.

Dawson, K. W., Meskhidze, N., Josset, D., and Gassó, S.: Spaceborne observations of the lidar ratio of marine aerosol, Atmos. Chem. Phys., 15, 3241-3255, https://doi.org/10.5194/acp-15-3241-2015, 2015.

De Leeuw, F., Sluyter, R., van Breugel, P., and Bogman, F.: Air Pollution by ozone in Europe in 1999 and the summer of 2000, European Environmental Agency Topic Report number 1/2001, EEA, Copenhagen, Denmark, 2001.

Delanoë, J. and Hogan, R. J.: A variational scheme for retrieving ice cloud properties from combined radar, lidar, and infrared

radiometer, J. Geophys. Res., 113, doi:10.1029/2007JD009000, 2008.

Dörnbrack, A., Stachlewska, I. S., Ritter, C., and Neuber, R.: Aerosol distribution around Svalbard during intense easterly winds, Atmos. Chem. Phys., 10, 1473-1490, https://doi.org/10.5194/acp-10-1473-2010, 2010.

Du, C., Liu, S., Yu, X., Li, X., Chen, C., Peng, Y., Dong, Y., Dong, Z., and Wang, F.: Urban boundary layer height characteristics and relationship with particulate matter mass concentrations in Xi'an, Central China, aerosol, Air Qual. Res., 13, 1598-1607, https://doi:10.4209/aaqr.2012.10.0274, 2013.

Di Biagio, C., Pelon, J., Ancellet, G., Bazureau, A., and Mariage, V.: Sources, load, vertical distribution, and fate of wintertime aerosol north of Svalbard from combined V4 CALIOP data, ground-based IAOOS lidar observations and trajectory analysis, J. Geophys. Res.-Atmos., 123, 1363–1383, https://doi.org/10.1002/2017JD027530, 2018.

Engelmann, R., Kanitz, T., Baars, H., Heese, B., Althausen, D., Skupin, A., Wandinger, U., Komppula, M., Stachlewska, I.S., Amiridis, V, Marinou, E., Mattis, I., Linné, H., and Ansmann, A.: The automated multiwavelength Raman polarization and water-vapor lidar Polly^{XT}: The neXT generation, Atmos. Meas. Tech., 9, 1767-1784, https://doi.org/10.5194/amt-9-1767-2016, 2016.

Fan, J., Wang, Y., Rosenfeld, D., and Liu, X.: Review of aerosol cloud interactions: Mechanisms, significance, and challenges, J. Atmos. Sci., 73, 4221–4252, https://doi.org/10.1175/JAS-D-16-0037.1, 2016.

Feingold, G., A. McComiskey, T. Yamaguchi, J. Johnson, K. Carslaw and K. S. Schmidt: New approaches to quantifying aerosol influence on the cloud radiative effect, Proc. Nat. Acad. Sci., 113, 5812-5819, https://doi.org/10.1073/pnas.1514035112, 2016.

Fiebig, M., Stohl, A., Wendisch, M., Eckhardt, S., and Petzold, A.: Dependence of solar radiative forcing of forest fire aerosol on ageing and state of mixture, Atmos. Chem. Phys., 3, 881-891, https://doi.org/10.5194/acp-3-881-2003, 2003.

Filip, L. and Stefan, S.: Study of the correlation between the near-ground PM10 mass concentration and the aerosol optical Depth, J. Atmos. Solar.-Terrestrial. Phys., 73, 1883-1889, https://doi.org/10.1016/j.jastp.2011.04.027, 2011.

Flentje, H., Heese, B., Reichardt, J., and Thomas, W.: Aerosol profiling using the ceilometer network of the German Meteorological Service, Atmos. Meas. Tech. Discuss., 3, 3643-3673, https://doi.org/10.5194/amtd-3-3643-2010, 2010.

Freudenthaler, V., Esselborn, M., Wiegner, M., Heese, B., Tesche, M., Ansmann, A., Müller, D., Althausen, D., Wirth, M., Fix, A., Ehret, G., Knippertz, P., Toledano, C., Gasteiger, J., Garhammer, M., and Seefeldner, M.: Depolarization ratio profiling at several wavelengths in pure Saharan dust during SAMUM 2006, Tellus B, 61, 165–179, https://doi:10.1111/j.1600-0889.2008.00396.x, 2009.

Freudenthaler, V., Linné, H., Chaikovski, A., Rabus, D., and Groß, S.: EARLINET lidar quality assurance tools, Atmos. Meas. Tech. Discuss., https://doi.org/10.5194/amt-2017-395, in review, 2018.

Foth, A., Kanitz, T., Engelmann, R., Baars, H., Radenz, M., Seifert, P., Barja, B., Fromm, M., Kalesse, H., and Ansmann, A.: Vertical aerosol distribution in the southern hemispheric midlatitudes as observed with lidar in Punta Arenas, Chile (53.2° S and 70.9° W), during ALPACA, Atmos. Chem. Phys., 19, 6217-6233, https://doi.org/10.5194/acp-19-6217-2019, 2019.

Fuzzi, S., Baltensperger, U., Carslaw, K., Decesari, S., Denier van der Gon, H., Facchini, M. C., Fowler, D., Koren, I., Langford, B., Lohmann, U., Nemitz, E., Pandis, S., Riipinen, I., Rudich, Y., Schaap, M., Slowik, J. G., Spracklen, D. V., Vignati, E.,

Wild, M., Williams, M., and Gilardoni, S.: Particulate matter, air quality and climate: lessons learned and future needs, Atmos. Chem. Phys., 15, 8217–8299, https://doi.org/10.5194/acp-15-8217-2015, 2015.

Gayatri, K., Patade, S., and Prabha, T. V.: Aerosol–Cloud interaction in deep convective clouds over the Indian Peninsula using spectral (bin) microphysics, J. Atmos. Sci., 74, 3145–3166, https://doi.org/10.1175/JAS-D-17-0034.1, 2017.

Gasteiger, J., and Freudenthaler, V.: Benefit of depolarization ratio at λ=1064 nm for the retrieval of the aerosol microphysics from lidar measurements, Atmos. Meas. Tech., 7, 3773-3781, https://doi.org/10.5194/amt-7-3773-2014, 2014.

Ghan, S. J., Wang, M., Zhang, S., Ferrachat, S., Gettleman, A., Griesfeller, J., Kipling, Z., Lohmann, U., Morrison, H., Neubauer, D., Partridge, D. G., Stier, P., Takemura, T., Wang, H., and Zhang, K.: Challenges in constraining anthropogenic aerosol effects on cloud radiative forcing using present-day spatiotemporal variability, P. Natl. Acad. Sci. 113, 5804–5811, https://doi.org/10.1073/pnas.1514036113, 2016.

Grund, C. J. and Eloranta, E. W.: University of Wisconsin High Spectral Resolution Lidar, Opt. Eng., 30, 6–12, 1991.

Groß, S., Tesche, M., Freudenthaler, V., Toledano, C., Wiegner, M., Ansmann, A., Althausen, D., and Seefeldner, M.: Characterization of Saharan dust, marine aerosol and mixtures of biomass-burning aerosol and dust by means of multi-wavelength depolarization and Raman lidar measurements during SAMUM 2, Tellus B: Chem. and Phys. Meteo., 63, 706-724, https://doi.org/10.1111/j.1600-0889.2011.00556.x, 2011.

Groß, S., Esselborn, M., Weinzierl, B., Wirth, M., Fix, A., and Petzold, A.: Aerosol classification by airborne high spectral resolution lidar observations, Atmos. Chem. Phys., 13, 2487–2505, https://doi:10.5194/acp-13-2487-2013, 2013.

Groß, S., Freudenthaler, V., Schepanski, K., Toledano, C., Schäfler, A., Ansmann, A., and Weinzierl, B.: Optical properties of long-range transported Saharan dust over Barbados as measured by dual-wavelength depolarization Raman lidar measurements, Atmos. Chem. Phys., 15, 11067–11080, https://doi.org/10.5194/acp-15-11067-2015, 2015.

Geiß, A., Wiegner, M., Bonn, B., Schäfer, K., Forkel, R., von Schneidemesser, E., Münkel, C., Chan, K. L., and Nothard, R.: Mixing layer height as an indicator for urban air quality?, Atmos. Meas. Tech., 10, 2969-2988, https://doi.org/10.5194/amt-10-2969-2017, 2017.

Giannakaki, E., Balis, D., Amiridis, V., and Zerefos, C.: Optical properties of different aerosol types: Seven years of combined Raman-elastic backscatter lidar measurements in Thessaloniki, Greece, Atmos. Meas. Tech., 3, 569-578, https://doi.org/10.5194/amt-3-569-2010, 2010.

Granados-Muñoz, M. J., Navas-Guzmán, F., Bravo-Aranda, J. A., Guerrero-Rascado, J. L., Lyamani, H., Valenzuela, A., Titos, G., Fernández-Gálvez, J., and Alados-Arboledas, L.: Hygroscopic growth of atmospheric aerosol particles based on active remote sensing and radiosounding measurements: selected cases in southeastern Spain, Atmos. Meas. Tech., 8, 705-718, https://doi.org/10.5194/amt-8-705-2015, 2015.

Giles, D. M., Sinyuk, A., Sorokin, M. G., Schafer, J. S., Smirnov, A., Slutsker, I., Eck, T. F., Holben, B. N., Lewis, J. R., Campbell, J. R., Welton, E. J., Korkin, S. V., and Lyapustin, A. I.: Advancements in the Aerosol Robotic Network (AERONET) Version 3 database – automated near-real-time quality control algorithm with improved cloud screening

for Sun photometer aerosol optical depth (AOD) measurements, Atmos. Meas. Tech., 12, 169-209, https://doi.org/10.5194/amt-12-169-2019, 2019.

Guo, J.-P., Zhang, X.-Y., Che, H.-Z., Gong, S.-L., An, X., Cao, C.-X., Guang, J., Zhang, H., Wang, Y.-Q., Zhang, X.-C., Xue, M., and Li, X.-W.: Correlation between PM concentrations and aerosol optical depth in eastern China, Atmos. Environ., 43, 5876–5886, https://doi.org/10.1016/j.atmosenv.2009.08.026, 2009.

Guo, H., Wang, Y., and Zhang, H.: Characterization of criteria air pollutants in Beijing during 2014–2015, Environ. Res., 154, 334-344, https://doi.org/10.1016/j.envres.2017.01.029, 2017.

Haarig, M., Ansmann, A., Gasteiger, J., Kandler, K., Althausen, D., Baars, H., Radenz, M., and Farrell, D. A.: Dry versus wet marine particle optical properties: RH dependence of depolarization ratio, backscatter, and extinction from multiwavelength lidar measurements during SALTRACE, Atmos. Chem. Phys., 17, 14199-14217, https://doi.org/10.5194/acp-17-14199-2017, 2017.

Haarig, M., Ansmann, A., Baars, H., Jimenez, C., Veselovskii, I., Engelmann, R., and Althausen, D.: Depolarization and lidar ratios at 355, 532, and 1064 nm and microphysical properties of aged tropospheric and stratospheric Canadian wildfire smoke, Atmos. Chem. Phys., 18, 11847-11861, https://doi.org/10.5194/acp-18-11847-2018, 2018.

Harrison, L., Michalsky, J., and Berndt, J.: Automated multifilter rotating shadow-band radiometer: An instrument for optical depth and radiation measurements, Appl. Opt., 33, 5118-5125, https://doi.org/10.1364/AO.33.005118, 1994.

Haeffelin, M., Angelini, F., Morille, Y., Martucci, G., Frey, S., Gobbi, G. P., Lolli, S., O'Dowd, C. D., Sauvage, L., XuerefRémy, I., Wastine, B., and Feist, D. G: Evaluation of mixing height retrievals from automatic profiling lidars and ceilometers in view of future integrated networks in Europe, Bound.-Lay. Meteorol., 143, 49–75, https://doi.org/10.1007/s10546-011-9643-z, 2012.

Hutchison, K. D., Faruqui, S. J., and Smith, S.: Improving correlations between MODIS aerosol optical thickness and ground-based PM2.5 observations through 3D spatial analyses, Atmos. Environ., 42, 530–543, https://doi.org/10.1016/j.atmosenv.2007.09.050, 2008.

Hu, Q., Goloub, P., Veselovskii, I., Bravo-Aranda, J.-A., Popovici, I. E., Podvin, T., Haeffelin, M., Lopatin, A., Dubovik, O., Pietras, C., Huang, X., Torres, B., and Chen, C.: Long-range-transported Canadian smoke plumes in the lower stratosphere over northern France, Atmos. Chem. Phys., 19, 1173-1193, https://doi.org/10.5194/acp-19-1173-2019, 2019.

He, Q., Li, C., Mao, J., Lau, A. K. H., and Chu, D.: Analysis of aerosol vertical distribution and variability in Hong Kong, J. Geophys. Res., 113, https://doi.org/10.1029/2008JD009778, 2008.

Heese, B., and Wiegner, M.: Vertical aerosol profiles from Raman polarization lidar observations during the dry season AMMA field campaign, J. Geophys. Res., 113, https://doi.org/10.1029/2007JD009487, 2008.

Holben, B. N., Eck, T. F., Slutsker, I., Tanre, D., Buis, J. P., Setzer, A., Vermote, E., Reagan, J. A., Kaufman, Y. J., Nakjima, T., Lavenu, F., Jankowiak, I., and Smirnov, A.: AERONET – A federated instrument network and data archive for aerosol characterization, Remote Sens. Environ., 66, 1–16, https://doi.org/10.1016/S0034-4257(98)00031-5, 1998.

Horvath, H., Alados Arboledas, L., and Olmo Reyes, F. J.: Angular scattering of the Sahara dust aerosol, Atmos. Chem. Phys., 18, 17735-17744, https://doi.org/10.5194/acp-18-17735-2018, 2018.

Iqbal, M.: An introduction to solar radiation, Acadamec Press, Ontario, 1983.

Iarlori, M., Madonna, F., Rizi, V., Trickl, T., and Amodeo, A.: Effective resolution concepts for lidar observations, Atmos. Meas. Tech., 8, 5157-5176, https://doi.org/10.5194/amt-8-5157-2015, 2015.

Illingworth, A. J., Barker, H. W., Beljaars, A., Ceccaldi, M., Chepfer, H., Clerbaux, N., Cole, J., Delanoë, J., Domenech, C., Donovan, D. P., Fukuda, S., Hirakata, M., Hogan, R. J., Huenerbein, A., Kollias, P., Kubota, T., Nakajima, T., Nakajima, T.Y., Nishizawa, T., Ohno, Y., Okamoto, H., Oki, R., Sato, K., Satoh, M., Shephard, M., Velázquez-Blázquez, A., Wandinger, U., Wehr, T., van Zadelhoff, G.-J.: The EarthCARE Satellite: The next step forward in global measurements of clouds, aerosol, precipitation and radiation, B. Am. Meteorol. Soc., 96, 1311–1332, doi:10.1175/BAMS-D-12-00227.1, 2015.

Janicka, L., Stachlewska, I. S., Veselovskii, I., and Baars, H.: Temporal variations in optical and microphysical properties of mineral dust and biomass burning aerosol derived from daytime Raman lidar observations over Warsaw, Poland, Atmos. Environ., 169, 162-174, https://doi.org/10.1016/j.atmosenv.2017.09.022, 2017.

Juda-Rezler K., Reizer, M., and Oudinet, J.P.: Determination and analysis of PM10 source apportionment during episodes of air pollution in Central Eastern European urban areas: The case of wintertime 2006, Atmos. Environ., 45(36), 6557-6566, https://doi.org/10.1016/j.atmosenv.2011.08.020, 2011.

Juda-Rezler, K., Reizer, M., Huszar, P., Krueger, B., Zanis, P., Syrakov, D., Katragkou, E., Trapp, W., Melas, D., Chervenkov, H., Tegoulias, I., and Halenka, T.: Modelling the effects of climate change on air quality over central and Eastern Europe: concept, evaluation and projections, Clim. Res., 53, 179–203, https://doi.org/10.3354/cr01072, 2012.

Jung, E., Albrecht, B. A., Feingold, G., Jonsson, H. H., Chuang, P., and Donaher, S. L.: Aerosol, clouds, and precipitation in the North Atlantic trades observed during the Barbados aerosol cloud experiment – Part 1: Distributions and variability, Atmos. Chem. Phys., 16, 8643-8666, https://doi.org/10.5194/acp-16-8643-2016, 2016.

Kaufman, Y. J., Tanré, D., and Boucher, O.: A satellite view of aerosol in the climate system, Nature, 419, 215, https://doi.org/10.1038/nature01091, 2002.

Koffi, B., Schulz, M., Breon, F. M., Dentener, F., Steensen, B. M., Griesfeller, J., Winker, D., Balkanski, Y., Bauer, S. E., Bellouin, N., Berntsen, T., Bian, H. S., Chin, M., Diehl, T., Easter, R., Ghan, S., Hauglustaine, D. A., Iversen, T., Kirkevag, A., Liu, X. H., Lohmann, U., Myhre, G., Rasch, P., Seland, O., Skeie, R. B., Steenrod, S. D., Stier, P., Tackett, J., Takemura, T., Tsigaridis, K., Vuolo, M. R., Yoon, J., and Zhang, K.: Evaluation of the aerosol vertical distribution in global aerosol models through comparison against CALIOP measurements: AeroCom phase II results, J. Geophys. Res.-Atmos., 121, 7254–7283, https://doi.org/10.1002/2015JD024639, 2016.

Kipling, Z., Stier, P., Johnson, C. E., Mann, G. W., Bellouin, N., Bauer, S. E., Bergman, T., Chin, M., Diehl, T., Ghan, S. J., Iversen, T., Kirkevåg, A., Kokkola, H., Liu, X., Luo, G., van Noije, T., Pringle, K. J., von Salzen, K., Schulz, M., Seland, Ø., Skeie, R. B., Takemura, T., Tsigaridis, K., and Zhang, K.: What controls the vertical distribution of aerosol? Relationships between process sensitivity in HadGEM3-UKCA and inter-model variation from AeroCom Phase II, Atmos. Chem. Phys., 16, 2221–2241, https://doi.org/10.5194/acp-16-2221-2016, 2016.

Lelieveld, J., Evans, J. S., Fnais, M., Giannadaki, D., and Pozzer, A.: The contribution of outdoor air pollution sources to

premature mortality on a global scale, Nature, 525, 367, https://doi.org/10.1038/nature15371, 2015.

Li, X., Ma, Y., Wang, Y., Liu, N., and Hong, Y.: Temporal and spatial analyses of particulate matter (PM10 and PM2. 5) and its relationship with meteorological parameters over an urban city in Northeast China, Atmos. Res., 198, 185-193, https://doi.org/10.1016/j.atmosres.2017.08.023, 2017.

5   Lisok, J., Rozwadowska, A., Pedersen, J. G., Markowicz, K. M., Ritter, C., Kaminski, J. W., Struzewska, J., Mazzola, M., Udisti, R., Becagli, S., and Gorecka, I.: Radiative impact of an extreme Arctic biomass-burning event, Atmos. Chem. Phys., 18, 8829–8848, https://doi.org/10.5194/acp-18-8829-2018, 2018.

Liu, Y., Franklin, M., Kahn, R., and Koutrakis, P.: Using aerosol optical thickness to predict ground-level PM2.5 concentrations in the St. Louis area: A comparison between MISR and MODIS, Remote Sens. Environ., 107, 33–44, 10   https://doi.org/10.1016/j.rse.2006.05.022, 2007.

Lolli, S., Madonna, F., Rosoldi, M., Campbell, J. R., Welton, E. J., Lewis, J. R., Gu, Y., and Pappalardo, G.: Impact of varying lidar measurement and data processing techniques in evaluating cirrus cloud and aerosol direct radiative effects, Atmos. Meas. Tech., 11, 1639-1651, https://doi.org/10.5194/amt-11-1639-2018, 2018.

Lolli S., Di Girolamo P.: Principal Component Analysis Approach to Evaluate Instrument Performances in Developing a Cost- 15   Effective Reliable Instrument Network for Atmospheric Measurements, Journal of Atmospheric and Oceanic Technology, Vol.32(9), 1642-1649, ISSN:1520-0426, 2015, https://doi.org/10.1175/JTECH-D-15-0085.1

Marinou, E., Amiridis, V., Binietoglou, I., Tsikerdekis, A., Solomos, S., Proestakis, E., Konsta D., Papagiannopoulos, N., Tsekeri, A., and Vlastou, G.: Three-dimensional evolution of Saharan dust transport towards Europe based on a 9-year EARLINET-optimized CALIPSO dataset, Atmos. Chem. Phys., 17, https://doi.org/10.5194/acp-17-5893-2017, 2017.

20   Markowicz, K., Chilinski, M.T., Lisok, J., Zawadzka, O., Stachlewska, I.S., Janicka, L., Rozwadowska, A., Makuch, P., Pakszys, P., Zielinski, T., Petelski, T., Posyniak, M., Pietruczuk, A., Szkop, A., and Westphal, D.L.: Study of aerosol optical properties during long-range transport of biomass burning from Canada to Central Europe in July 2013, J. Aeros. Sci., 101, 156-173, https://doi.org/10.1016/j.jaerosci.2016.08.006, 2016.

Masonis, S. J., Anderson, T. L., Covert, D. S., Kapustin, V., Clarke, A. D., Howell, S., and Moore, K.: A study of the 25   extinction-to-backscatter ratio of marine aerosol during the shoreline environment aerosol study, J. Atmos. Ocean. Techn., 20, 1388-1402, https://doi.org/10.1175/1520-0426(2003)020<1388:ASOTER>2.0.CO;2, 2003.

Matthias, V., Balis, D., Bösenberg, J., Eixmann, R., Iarlori, M., Komguem, L., Mattis, I., Papayannis, A., Pappalardo, G., and Perrone, M.: Vertical aerosol distribution over Europe: Statistical analysis of Raman lidar data from 10 European aerosol research lidar network (EARLINET) stations, J. Geophys. Res., 109, https://doi.org/10.1029/2004JD004638, 30   2004.

Mattis, I., Ansmann, A., Müller, D., Wandinger, U., and Althausen, D.: Multiyear aerosol observations with dual-wavelength Raman lidar in the framework of EARLINET, J. Geophys. Res., 109, https://doi.org/10.1029/2004JD004600, 2004.

Masson-Delmotte, V., P. Zhai, H.-O. Pörtner, D. Roberts, J. Skea, P.R. Shukla, A. Pirani, W. Moufouma-Okia, C. Péan, R. Pidcock, S. Connors, J.B.R. Matthews, Y. Chen, X. Zhou, M.I. Gomis, E. Lonnoy, T. Maycock, M. Tignor, and T. Waterfield.:

IPCC, 2018: Global Warming of 1.5°C. An IPCC Special Report on the impacts of global warming of 1.5°C above pre-industrial levels and related global greenhouse gas emission pathways, in the context of strengthening the global response to the threat of climate change, sustainable development, and efforts to eradicate poverty.

Müller, D., Ansmann, A., Mattis, I., Tesche, M., Wandinger, U., Althausen, D., and Pisani, G.: Aerosol- type- dependent lidar ratios observed with Raman lidar, J. Geophys. Res., 112, https://doi.org/10.1029/2006JD008292, 2007.

Mona, L., Amodeo, A., D'Amico, G., Giunta, A., Madonna, F., and Pappalardo, G.: Multi-wavelength Raman lidar observations of the Eyjafjallajökull volcanic cloud over Potenza, southern Italy, Atmos. Chem. Phys., 12, 2229-2244, https://doi.org/10.5194/acp-12-2229-2012, 2012.

Navas-Guzmán, F., Martucci, G., Collaud Coen, M., Granados-Muñoz, M. J., Hervo, M., Sicard, M., and Haefele, A.: Characterization of aerosol hygroscopicity using Raman lidar measurements at the EARLINET station of Payerne, Atmos. Chem. Phys., 19, 11651–11668, https://doi.org/10.5194/acp-19-11651-2019, 2019.

Nicolae, D., Vasilescu, J., Talianu, C., Binietoglou, I., Nicolae, V., Andrei, S., and Antonescu, B.: A neural network aerosol-typing algorithm based on lidar data, Atmos. Chem. Phys., 18, 14511-14537, https://doi.org/10.5194/acp-18-14511-2018, 2018.

Nemuc, A., Vasilescu, J., Talianu, C., Belegante, L., and Nicolae, D.: Assessment of aerosol's mass concentrations from measured linear particle depolarization ratio (vertically resolved) and simulations, Atmos. Meas. Tech., 6, 3243-3255, https://doi.org/10.5194/amt-6-3243-2013, 2013.

Nemuc, A., Stachlewska, I. S., Valilescu, J., Górska, A., Nicolae, D., and Talianu, C.: Optical Properties of Long-Range Transported Volcanic Ash over Romania and Poland During Eyjafjallajökull Eruption in 2010, Acta Geophys., 62, 350–366 doi:10.2478/s11600-013-0180-7, 2014.

Ortiz-Amezcua, P., Guerrero-Rascado, J. L., Granados-Muñoz, M. J., Benavent-Oltra, J. A., Böckmann, C., Samaras, S., Stachlewska, I. S., Janicka, Ł., Baars, H., and Bohlmann, S.: Microphysical characterization of long-range transported biomass burning particles from North America at three EARLINET stations, Atmos. Chem. Phys., 17, 5931-5946, https://doi.org/10.5194/acp-17-5931-2017, 2017.

Pan, X., Chin, M., Gautam, R., Bian, H., Kim, D., Colarco, P. R., Diehl, T. L., Takemura, T., Pozzoli, L., Tsigaridis, K., Bauer, S., and Bellouin, N.: A multi-model evaluation of aerosol over South Asia: common problems and possible causes, Atmos. Chem. Phys., 15, 5903–5928, https://doi.org/10.5194/acp-15-5903-2015, 2015.

Papagiannopoulos, N., Mona, L., Alados-Arboledas, L., Amiridis, V., Baars, H., Binietoglou, I., Bortoli, D., D'Amico, G., Giunta, A., Guerrero-Rascado, J. L., Schwarz, A., Pereira, S., Spinelli, N., Wandinger, U., Wang, X., and Pappalardo, G.: CALIPSO climatological products: evaluation and suggestions from EARLINET, Atmos. Chem. Phys., 16, 2341–2357, https://doi.org/10.5194/acp-16-2341-2016, 2016.

Papagiannopoulos, N., Mona, L., Amodeo, A., D'Amico, G., Gumà Claramunt, P., Pappalardo, G., Alados-Arboledas, L., Guerrero-Rascado, J. L., Amiridis, V., Kokkalis, P., Apituley, A., Baars, H., Schwarz, A., Wandinger, U., Binietoglou, I., Nicolae, D., Bortoli, D., Comerón, A., Rodríguez-Gómez, A., Sicard, M., Papayannis, A., and Wiegner, M.: An automatic

observation-based aerosol typing method for EARLINET, Atmos. Chem. Phys., 18, 15879-15901, https://doi.org/10.5194/acp-18-15879-2018, 2018.

Papayannis, A., Amiridis, V., Mona, L., Tsaknakis, G., Balis, D., Bosenberg, J., Chaikovski, A., De Tomasi, F., Grigorov, I., Mattis, I., Mitev, V., Muller, D., Nickovic, S., Perez, C., Pietruczuk, A., Pisani, G., Ravetta, F., Rizi, V., Sicard, M., Trickl, T., Wiegner, M., Gerding, M., Mamouri, R. E., D'Amico, G., and Pappalardo, G.: Systematic lidar observations of Saharan dust over Europe in the frame of EARLINET (2000–2002), J. Geophys. Res., 113, D10204, https://doi.org/10.1029/2007JD009028, 2008.

Pappalardo, G., Amodeo, A., Apituley, A., Comeron, A., Freudenthaler, V., Linné, H., Ansmann, A., Bösenberg, J., D'Amico, G., and Mattis, I.: EARLINET: Towards an advanced sustainable European aerosol lidar network, Atmos. Meas. Tech., 7, 2389-2409, https://doi.org/10.5194/amt-7-2389-2014, 2014.

Perrone, M. R., De Tomasi, F., and Gobbi, G. P.: Vertically resolved aerosol properties by multi-wavelength lidar measurements, Atmos. Chem. Phys., 14, 1185-1204, https://doi.org/10.5194/acp-14-1185-2014, 2014.

Petters, M. D., Carrico, C. M., Kreidenweis, S. M., Prenni, A. J., DeMott, P. J., Collett, J. L., and Moosmüller, H.: Cloud condensation nucleation activity of biomass burning aerosol, J. Geophys. Res., 114, https://doi.org/10.1029/2009JD012353, 2009.

Pope, S. B.: Turbulent Flows. Cambridge University Press, 771pp, UK, 2000.

Pósfai, M., Gelencsér, A., Simonics, R., Arató, K., Li, J., Hobbs, P.V., and Buseck, P.R.: Atmospheric tar balls: Particles from biomass and biofuel burning, J. Geophys. Res., 109, https://doi.org/10.1029/2003JD004169, 2004.

Popovici, I. E., Goloub, P., Podvin, T., Blarel, L., Loisil, R., Unga, F., Mortier, A., Deroo, C., Victori, S., Ducos, F., Torres, B., Delegove, C., Choël, M., Pujol-Söhne, N., and Pietras, C.: Description and applications of a mobile system performing on-road aerosol remote sensing and in situ measurements, Atmos. Meas. Tech., 11, 4671-4691, https://doi.org/10.5194/amt-11-4671-2018, 2018.

Proestakis, E., Amiridis, V., Marinou, E., Binietoglou, I., Ansmann, A., Wandinger, U., Hofer, J., Yorks, J., Nowottnick, E., Makhmudov, A., Papayannis, A., Pietruczuk, A., Gialitaki, A., Apituley, A., Szkop, A., Muñoz Porcar, C., Bortoli, D., Dionisi, D., Althausen, D., Mamali, D., Balis, D., Nicolae, D., Tetoni, E., Liberti, G. L., Baars, H., Mattis, I., Stachlewska, I. S., Voudouri, K. A., Mona, L., Mylonaki, M., Perrone, M. R., Costa, M. J., Sicard, M., Papagiannopoulos, N., Siomos, N., Burlizzi, P., Pauly, R., Engelmann, R., Abdullaev, S., and Pappalardo, G.: EARLINET evaluation of the CATS Level 2 aerosol backscatter coefficient product, Atmos. Chem. Phys., 19, 11743–11764, https://doi.org/10.5194/acp-19-11743-2019, 2019.

Qin, K., Zou, J., Guo, J., Lu, M., Bilal, M., Zhang, K., Ma, F and Zhang, Y.: Estimating PM1 concentrations from MODIS over Yangtze River Delta of China during 2014–2017. Atmos. Environ., 195, 149-158. https://doi.org/10.1016/j.atmosenv.2018.09.054, 2018.

Reizer, M., Juda-Rezler, K.: Explaining the high PM_{10} concentrations observed in Polish urban areas, Air Qual. Atmos Health., 9 (5), 517-531, https://doi.org/10.1007/s11869-015-0358-z. 2015.

Rost, J., Holst, T., Sähn, E., Klingner, M., Anke, K., Ahrens, D., and Mayer, H.: Variability of PM10 concentrations

dependent on meteorological conditions, Intern. J. Environ. Poll., 36, 3-18, https://doi.org/10.1504/IJEP.2009.021813, 2009.

Sakai, T., Nagai, T., Zaizen, Y., and Mano, Y.: Backscattering linear depolarization ratio measurements of mineral, sea-salt, and ammonium sulfate particles simulated in a laboratory chamber, Appl. Opt., 49, 4441-4449, https://doi.org/10.1364/AO.49.004441, 2010.

Seinfeld, J. H., Bretherton, C., Carslaw, K. S., Coe, H., DeMott, P. J., Dunlea, E. J., Feingold, G., Ghan, S., Guenther, A. B., Kahn, R., Kraucunas, I., Kreidenweis, S. M., Molina, M. J., Nenes, A., Penner, J. E., Prather, K. A., Ramanathan, V., Ramaswamy, V., Rasch, P. J., Ravishankara, A. R., Rosenfeld, D., Stephens, G., and Wood, R.: Improving our fundamental understanding of the role of aerosol–cloud interactions in the climate system, P. Natl. Acad. Sci., 113, 5781–5790, https://doi.org/10.1073/pnas.1514043113, 2016.

Schmeisser, L., Andrews, E., Ogren, J. A., Sheridan, P., Jefferson, A., Sharma, S., Kim, J. E., Sherman, J. P., Sorribas, M., Kalapov, I., Arsov, T., Angelov, C., Mayol-Bracero, O. L., Labuschagne, C., Kim, S.-W., Hoffer, A., Lin, N.-H., Chia, H.-P., Bergin, M., Sun, J., Liu, P., and Wu, H.: Classifying aerosol type using in situ surface spectral aerosol optical properties, Atmos. Chem. Phys., 17, 12097-12120, https://doi.org/10.5194/acp-17-12097-2017, 2017.

Sicard, M., Rocadenbosch, F., Reba, M. N. M., Comerón, A., Tomás, S., García-Vízcaino, D., Batet, O., Barrios, R., Kumar, D., and Baldasano, J. M.: Seasonal variability of aerosol optical properties observed by means of a Raman lidar at an EARLINET site over Northeastern Spain, Atmos. Chem. Phys., 11, 175-190, https://doi.org/10.5194/acp-11-175-2011, 2011.

Siomos, N., Balis, D. S., Poupkou, A., Liora, N., Dimopoulos, S., Melas, D., Giannakaki, E., Filioglou, M., Basart, S., and Chaikovsky, A.: Investigating the quality of modeled aerosol profiles based on combined lidar and sunphotometer data, Atmos. Chem. Phys., 17, 7003-7023, https://doi.org/10.5194/acp-17-7003-2017, 2017.

Siomos, N., Balis, D. S., Voudouri, K. A., Giannakaki, E., Filioglou, M., Amiridis, V., Papayannis, A., and Fragkos, K.: Are EARLINET and AERONET climatologies consistent? The case of Thessaloniki, Greece, Atmos. Chem. Phys., 18, 11885-11903, https://doi.org/10.5194/acp-18-11885-2018, 2018.

Stein, A. F., Draxler, R. R., Rolph, G. D., Stunder, B. J. B., Cohen, M. D., and Ngan, F.: NOAA's HYSPLIT Atmospheric Transport and Dispersion Modeling System, B. Am. Meteorol. Soc., 96, 2059–2077, https://doi.org/10.1175/BAMS-D-14-00110.1, 2015.

Stachlewska, I., Piądłowski, M., Migacz, S., Szkop, A., Zielińska, A., Swaczyna, P.: Ceilometer observations of the boundary layer over Warsaw, Poland, Acta Geophys. 60, 1386-1412. https://doi.org/10.2478/s11600-012-0054-4, 2012.

Stachlewska, I. S., Costa-Surós, M., and Althausen, D.: Raman lidar water vapour profiling over Warsaw, Poland, Atmos. Res., 194, 258-267, https://doi.org/10.1016/j.atmosres.2017.05.004, 2017a.

Stachlewska, I.S., Zawadzka, O., and Engelmann, R.: Effect of heat wave conditions on aerosol optical properties derived from satellite and ground-based remote sensing over Poland, Remote Sens., 9, 1199, https://doi.org/10.3390/rs9111199, 2017b.

Stachlewska, I. S., Samson, M., Zawadzka, O., Harenda, K. M., Janicka, L., Poczta, P., Szczepanik, D., Heese, B., Wang, D., and Borek, K. Tetoni, E., Proestakis, E., Siomos, N., Nemuc, A., Chojnicki, B.H., Markowicz, K.M., Pietruczuk, A., Szkop, A., Althausen, D., Stebel, K., Schuettemeyer, D., and Zehner, C.: Modification of local urban aerosol properties by long-range transport of biomass burning aerosol, Remote Sens., 10, 412, https://doi.org/10.3390/rs10030412, 2018.

5   Stocker, T., Qin, D., Plattner, G., Tignor, M., Allen, S., Boschung, J., Nauels, A., Xia, Y., Bex, V., and Midgley, P.: IPCC, 2013: Climate Change 2013: The Physical Science Basis. Contribution of Working Group I to the Fifth Assessment Report of the Intergovernmental Panel on Climate Change, Cambridge Univ. Press, Cambridge, UK, and New York, 1535 pp., 2013.

Szczepanik, D. and Markowicz, K.: The relation between columnar and surface aerosol optical properties in a background
10   environment, Atmos. Poll. Res., 9, 246-256, https://doi.org/10.1016/j.apr.2017.10.001, 2018.

Szczepanik, D., Tetoni, E., Wang, D., and Stachlewska, I.: Lidar Based Separation of Polluted Dust Observed over Warsaw (Case Study on 09 August 2013), the 29th International Laser Radar Conference, Hefei, China, 24-28 June, 1-5, 2019.

Szkop, A. and Pietruczuk, A.: Analysis of aerosol transport over southern Poland in August 2015 based on a synergy of remote sensing and backward trajectory techniques, J. Appl. Remote. Sens., 11, 016039, https://doi.org/10.1117/
15   1.JRS.11.016039, 2017.

Schäfer, K., Emeis, S., Hoffmann, H., and Jahn, C.: Influence of mixing layer height upon air pollution in urban and sub-urban areas, Meteorol. Z., 15 (12), 647-658, https://doi.org/10.1127/0941-2948/2006/0164, 2006.

Schaap, M., Apituley, A., Timmermans, R. M. A., Koelemeijer, R. B. A., and de Leeuw, G.: Exploring the relation between aerosol optical depth and PM2.5 at Cabauw, the Netherlands, Atmos. Chem. Phys., 9, 909-925, https://doi.org/10.5194/acp-9-
20   909-2009, 2009.

Sharma, A., Mandal, T., Sharma, S., Shukla, D., and Singh, S.: Relationships of surface ozone with its precursors, particulate matter and meteorology over Delhi, J. Atmos. Chem., 74, 451-474, https://doi.org/10.1007/s10874-016-9351-7, 2017.

Stull, R. B.: An Introduction to Boundary Layer Meteorology, Kluwer Academic Publishers, Dordrecht, Netherlands, 1988.

The EARLINET publishing group 2000-2015.: EARLINET All 2000-2015. World Data Center for Climate (WDCC) at
25   DKRZ. https://doi.org/10.1594/WDCC/EARLINET_All_2000-2015, 2018.

Tian, P., Cao, X., Zhang, L., Sun, N., Sun, L., Logan, T., Shi, J., Wang, Y., Ji, Y., Lin, Y., Huang, Z., Zhou, T., Shi, Y., and Zhang, R.: Aerosol vertical distribution and optical properties over China from long-term satellite and ground-based remote sensing, Atmos. Chem. Phys., 17, 2509-2523, https://doi.org/10.5194/acp-17-2509-2017, 2017.

Trickl, T., Vogelmann, H., Flentje, H., and Ries, L.: Stratospheric ozone in boreal fire plumes – the 2013 smoke season over
30   central Europe, Atmos. Chem. Phys., 15, 9631-9649, https://doi.org/10.5194/acp-15-9631-2015, 2015.

Trippetta, S., Sabia, S., and Caggiano, R.: Fine aerosol particles (PM1): Natural and anthropogenic contributions and health risk assessment, Air Qual. Atmos. Hlth., 9, 621–629, https://doi.org/10.1007/s11869-015-0373-0, 2016.

Tang, I. N.: Chemical and size effects of hygroscopic aerosol on light scattering coefficients, J. Geophys. Res., 101, 19245–19250, https://doi.org/10.1029/96JD03003, 1996.

Veselovskii, I., Kolgotin, A., Griaznov, V., Müller, D., Wandinger, U., and Whiteman, D.N.: Inversion with regularization for the retrieval of tropospheric aerosol parameters from multiwavelength lidar sounding, Appl. Opt., 41, 3685–3699, https://doi.org/10.1364/AO.41.003685, 2002.

Wałaszek, K., Kryza, M., and Werner, M.: The role of precursor emissions on ground level ozone concentration during summer season in Poland, J. Atmos. Chem., 75, 181-204, https://doi.org/10.1007/s10874-017-9371-y, 2018.

Wandinger, U., Freudenthaler, V., Baars, H., Amodeo, A., Engelmann, R., Mattis, I., Groß, S., Pappalardo, G., Giunta, A., D'Amico, G., Chaikovsky, A., Osipenko, F., Slesar, A., Nicolae, D., Belegante, L., Talianu, C., Serikov, I., Linné, H., Jansen, F., Apituley, A., Wilson, K. M., de Graaf, M., Trickl, T., Giehl, H., Adam, M., Comerón, A., Muñoz-Porcar, C., Rocadenbosch, F., Sicard, M., Tomás, S., Lange, D., Kumar, D., Pujadas, M., Molero, F., Fernández, A. J., Alados-Arboledas, L., Bravo-Aranda, J. A., Navas-Guzmán, F., Guerrero-Rascado, J. L., Granados-Muñoz, M. J., Preißler, J., Wagner, F., Gausa, M., Grigorov, I., Stoyanov, D., Iarlori, M., Rizi, V., Spinelli, N., Boselli, A., Wang, X., Lo Feudo, T., Perrone, M.R., De Tomasi, F., and Burlizzi, P.: EARLINET instrument intercomparison campaigns: overview on strategy and results, Atmos. Meas. Tech., 9, 1001-1023, https://doi.org/10.5194/amt-9-1001-2016, 2016.

Wang, D., Stachlewska, I. S., Song, X., Heese, B., and A.Nemuc.: Variability of boundary layer over an urban continental site based on 10 years of active remote sensing observations in Warsaw, Remote Sens., in review, 2019.

Wang, J. and Christopher, S. A.: Intercomparison between satellite-derived aerosol optical thickness and PM2.5 mass: Implications for air quality studies, Geophys. Res. Lett., 30, 2095, https://doi.org/10.1029/2003GL018174, 2003.

Wolff, H., Perry, L.: Policy monitor: Trends in clean air legislation in Europe: Particulate matter and low emission zones. Rev. Environ. Econ. Policy, 4, 293-308,https://doi.org/10.1093/reep/req008, 2010.

Winker, D. M., Hunt, W. H., and McGill, M. J.: Initial performance assessment of CALIOP, Geophys. Res. Lett., 34, L19803, https://doi.org/10.1029/2007GL030135, 2007.

Xie, C., Nishizawa, T., Sugimoto, N., Matsui, I., and Wang, Z.: Characteristics of aerosol optical properties in pollution and Asian dust episodes over Beijing, China, Appl. Opt., 47, 4945-4951, https://doi.org/10.1364/AO.47.004945, 2008.

Zawadzka, O., Markowicz, K., Pietruczuk, A., Zielinski, T., and Jaroslawski, J.: Impact of urban pollution emitted in Warsaw on aerosol properties, Atmos. Environ., 69, 15-28, https://doi.org/10.1016/j.atmosenv.2012.11.065, 2013.

Zhang, H., Wang, Y., Hu, J., Ying, Q., and Hu, X.-M.: Relationships between meteorological parameters and criteria air pollutants in three megacities in China, Environ. Res., 140, 242-254, https://doi.org/10.1016/j.envres.2015.04.004, 2015.

Zang, Z. L., Wang, W. Q., You, W., Li, Y., Ye, F., and Wang, C. M.: Estimating ground-level PM2.5 concentrations in Beijing, China using aerosol optical depth and parameters of the temperature inversion layer, Sci. Total Environ., 575, 1219–1227, https://doi.org/10.1016/j.scitotenv.2016.09.186, 2017.

Zheng, S., Pozzer, A., Cao, C. X., and Lelieveld, J.: Long-term (2001–2012) concentrations of fine particulate matter ($PM_{2.5}$) and the impact on human health in Beijing, China, Atmos. Chem. Phys., 15, 5715-5725, https://doi.org/10.5194/acp-15-5715-2015, 2015.

Table 1. Literature review based on the values of the lidar derived particle optical properties which used for the interpretation of aerosol measured over the RS-Lab in Warsaw. The listed properties are assessed in each aerosol layer based on a manual approach in a combination with case-to-case air-mass transport analyses.

	LR [sr]		δ [%]		ÅE	RH	Air-mass transport *	No. of cases (in ABL) [%]
	355	532	355	532	(355/532)	[%]		
Anthropogenic pollution	50-65	33-72	3-6	3-11	0.7-1.8	50-90	Local (Warsaw) Advective (Western Europe)	151 (61%)
Biomass burning	50-95	60-90	2-6	4-12	0.8-2.0	60-80	Advective (Eastern Europe, North America)	34 (14%)
Pollen	50-75	46-69	5-17	6-20	---	< 50	Local	16 (7%)
Arctic marine	16-30	18-26	1-7	1-11	-0.6-0.7	---	Advective (Arctic, subarctic)	14 (5%)
Dust	50-70	45-65	24-29	25-43	0.1-1.5	20-40	Advective (Africa)	0
Undefined Mixtures								31 (13%)

* Calculations up to 10 days backward-trajectories for aerosol layers in the free troposphere and in the boundary layer, assessment of possible source of aerosol by interpreting it against satellite data (MODIS, MSG, CALIPSO) and model outputs (NAAPS).

Table 2. Mean values of the aerosol optical properties with standard deviations derived within atmospheric boundary layer (ABL) from PollyXT lidar at the EARLINET site in Warsaw for measurements at 355 and 532 nm conducted fopr period of July-September of 2013, 2015, and 2016. Symbols denote: particle extinction coefficient (α), particle backscatter coefficient (β), aerosol optical depth (AOD), lidar ratio (LR), linear particle depolarization ratio (δ), Ångström exponent (ÅE) and atmospheric boundary layer height (ABLH). Mean values are obtained for different time of day with respect to the boundary layer type.

	λ (nm)	α_{ABL} (Mm^{-1})	β_{ABL} (Mm^{-1}sr^{-1})	AOD_{ABL}	LR_{ABL} (sr)	δ_{ABL}	$ÅE_{ABL}$	$ABLH$ (km)
Entire time (ET)								
WML, RL, MTL (246 cases)	355	142 ±68	3.1±1.2	0.20±0.10	48±17	0.02±0.01	1.54±0.37	1.33±0.36
	532	83 ±43	2.2±0.7	0.11±0.06	41±15	0.05±0.01		
Nocturnal time (NT) [21:00-2:00 UTC]								
NL (113 cases)	355	129±56	3.0±1.1	0.11±0.04	44±12	0.02±0.01	1.58±0.36	0.76±0.12
	532	69±39	1.9±0.7	0.07±0.02	38±12	0.05±0.01		
RL (105 cases)	355	137±53	3.1±1.0	0.18±0.08	47±15	0.02±0.01	1.61±0.38	1.34±0.17
	532	75±37	2.3±1.0	0.11±0.05	40±13	0.04±0.01		
Transition time (TT) during Sunrise [3:00-8:00 UTC] & Sunset [16:00-20:00 UTC]								
MTL (37 cases)	355	128±54	3.8±1.1	0.11±0.03	37±14	0.02±0.01	1.53±0.30	0.70±0.10
	532	73±35	2.3±0.6	0.06±0.02	32±13	0.04±0.01		
WML (63 cases)	355	163 ±63	2.8±1.1	0.24±0.01	55 ±18	0.02±0.01	1.37±0.34	1.60±0.38
	532	96 ±49	1.9±0.8	0.14±0.05	49±16	0.05±0.02		

Table 3. Mean daytime (3:00-19:00 UTC) aerosol optical depth (AOD) and Ångström exponent (ÅE) with standard deviations derived within atmospheric boundary layer at 355 and 532 nm from PollyXT lidar at the EARLINET site in Warsaw and in atmospheric column measured by MFR-7 shadowband radiometer (415 and 500 nm) at the PolandAOD-NET site in Warsaw. For reference the mean values derived from Version 3 Level 2.0 CE318 CIMEL (380 and 500 nm) at the AERONET site in Belsk are given. The AOD$_{CL}$ of CE318 and MFR-7 were scaled to the lidar wavelength (respectively 355 and 532 nm) using Ångström law. The mean values were obtained for July-September of 2013, 2015, 2016 when instruments operated simultaneously (41 cases). In brackets, the mean values derived for cases with no aerosol in the free troposphere (12 cases), as given in EARLINET/ACTRIS Data Base.

	AOD	AOD	ÅE(355/532)	ÅE(380/500)	ÅE(415/500)
AERONET Belsk (columnar) reference site CE318 photometer					
All cases	**355 nm**	**532nm**			
(no FT aerosol)	0.41±0.17	0.23±0.09	1.49±0.23		
	(0.28±0.12)	*(0.16±0.06)*	*(1.57±0.10)*		
	380 nm	**500nm**			
	0.36±0.16	0.24±0.12		1.51±0.23	
	(0.26±0.10)	*(0.19±0.08)*		*(1.60±0.13)*	
PolandAOD Warsaw (columnar) MFR-7 shadowband radiometer					
All cases	**355 nm**	**532 nm**			
(no FT aerosol)	0.45±0.17	0.25±0.11	1.56±0.21		
	(0.30±0.09)	*(0.15±0.06)*	*(1.71±0.17)*		
	415 nm	**500 nm**			
	0.36±0.15	0.27±0.12			1.50±0.31
	(0.26±0.08)	*(0.17±0.07)*			*(1.66±0.35)*
EARLINET Warsaw (within aerosol boundary) PollyXT-UW Raman lidar					
All cases	**355nm**	**532nm**			
(no FT aerosol)	0.20±0.06	0.13±0.03	1.53±0.23		
	(0.16±0.08)	*(0.10±0.03)*	*(1.60±0.15)*		
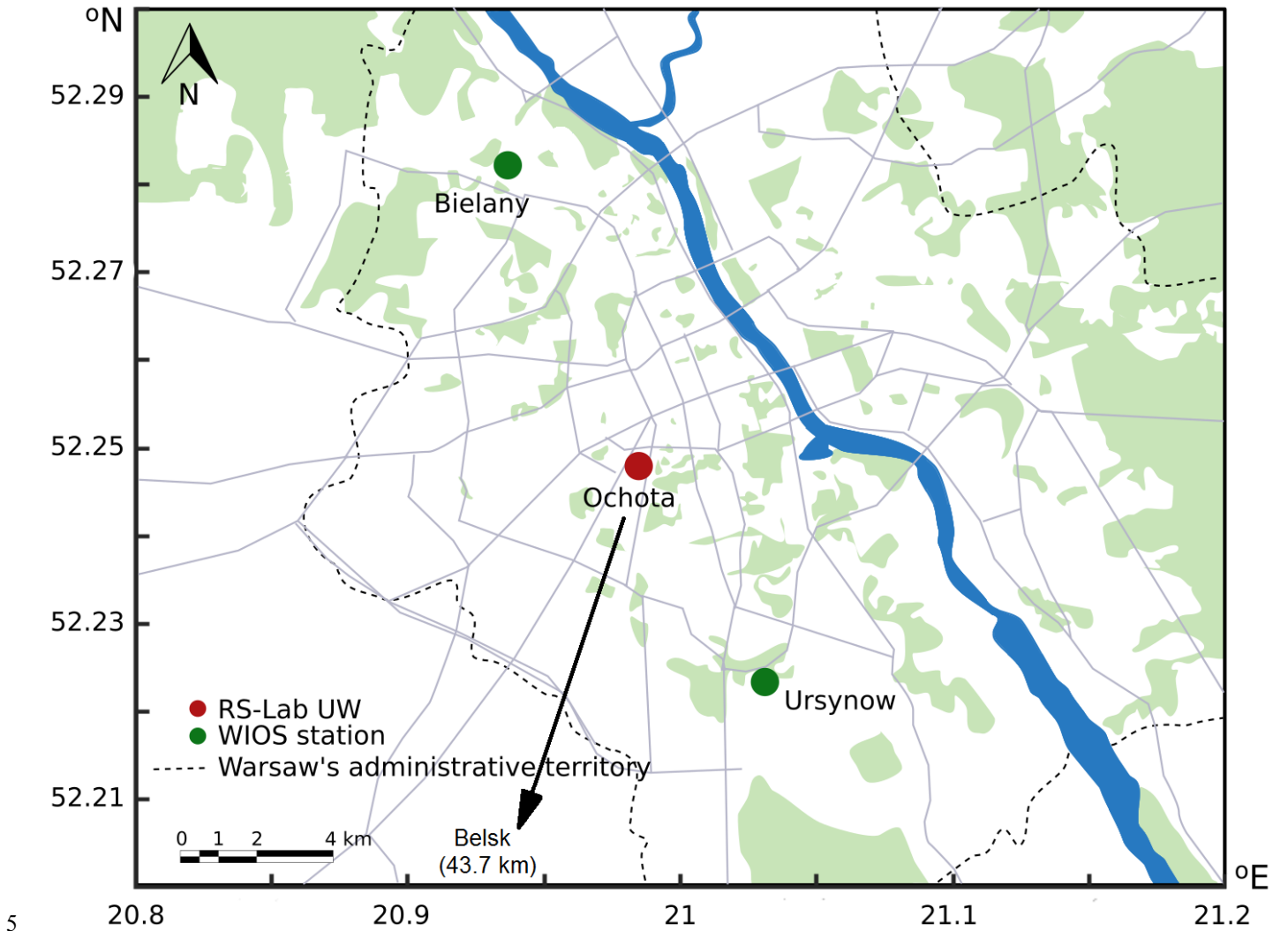
Figure 1. The location of the Remote Sensing Laboratory at UW Ochota Campus in Warsaw, Poland (in red), the WIOS monitoring stations in Ursynow and Bielany (in green), and the IGF-PAS Observatory in Belsk (arrow).
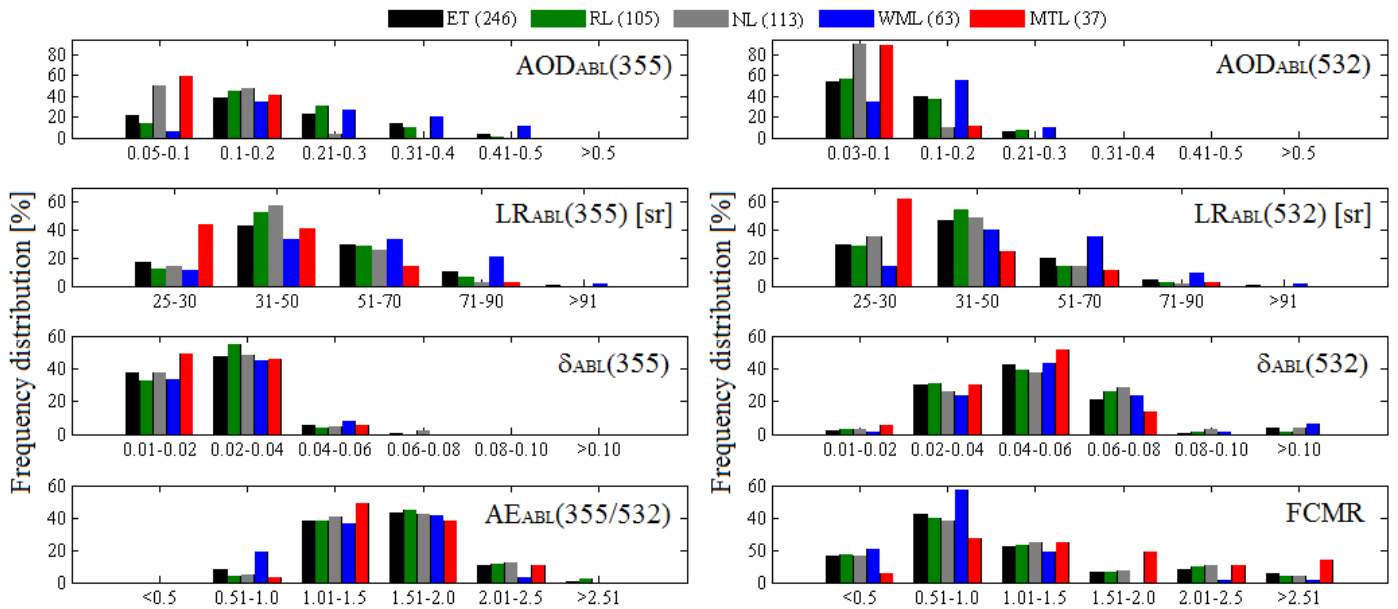
Figure 2. Frequency distribution of aerosol optical depth (AOD), lidar ratio (LR), linear particle depolarization ratio (δ) and Ångström exponent (ÅE) at 355 and 532 nm derived within atmospheric boundary layer at the EARLINET/ACTRIS lidar site in Warsaw for period of July-September 2013, 2015, 2016. Corresponding fine to coarse mass ratio (FCMR) derived from measurements of surface particulate matter with an aerodynamic diameter below 10μm (PM_{10}) and below 2.5μm ($PM_{2.5}$) at the WIOS site in Warsaw-Ursynow. The period of measurement is divided to the entire time (ET; 24 h), the nocturnal time (NT; 22:00-2:00 UTC, including the residual boundary layer RL and the nocturnal boundary layer NL), and the transition time (TT; after sunrise at 03:00-8:00 for the morning transition layer MTL and before sunset at 16:00-20:00 UTC for the well-mixed boundary layer WML).

Figure 3. Intercomparison of hourly averaged clear-sky daytime aerosol optical depth measured within the atmospheric column (AOD$_{CL}$) with CE318 at the AERONET site in Warsaw (Version 3 Level 2.0 data) and the MFR-7 shadowband radiometer at the PolandAOD-NET site in Warsaw (Level 1.5 data). Note a high agreement obtained for both wavelengths for a month (July 2018) of collocated measurements (instruments in a distance of 3 m at the same altitude) at the RS-Lab in Warsaw. The AOD$_{CL}$ at 415 nm from MFR-7 was scaled to 380 nm using Ångström law.
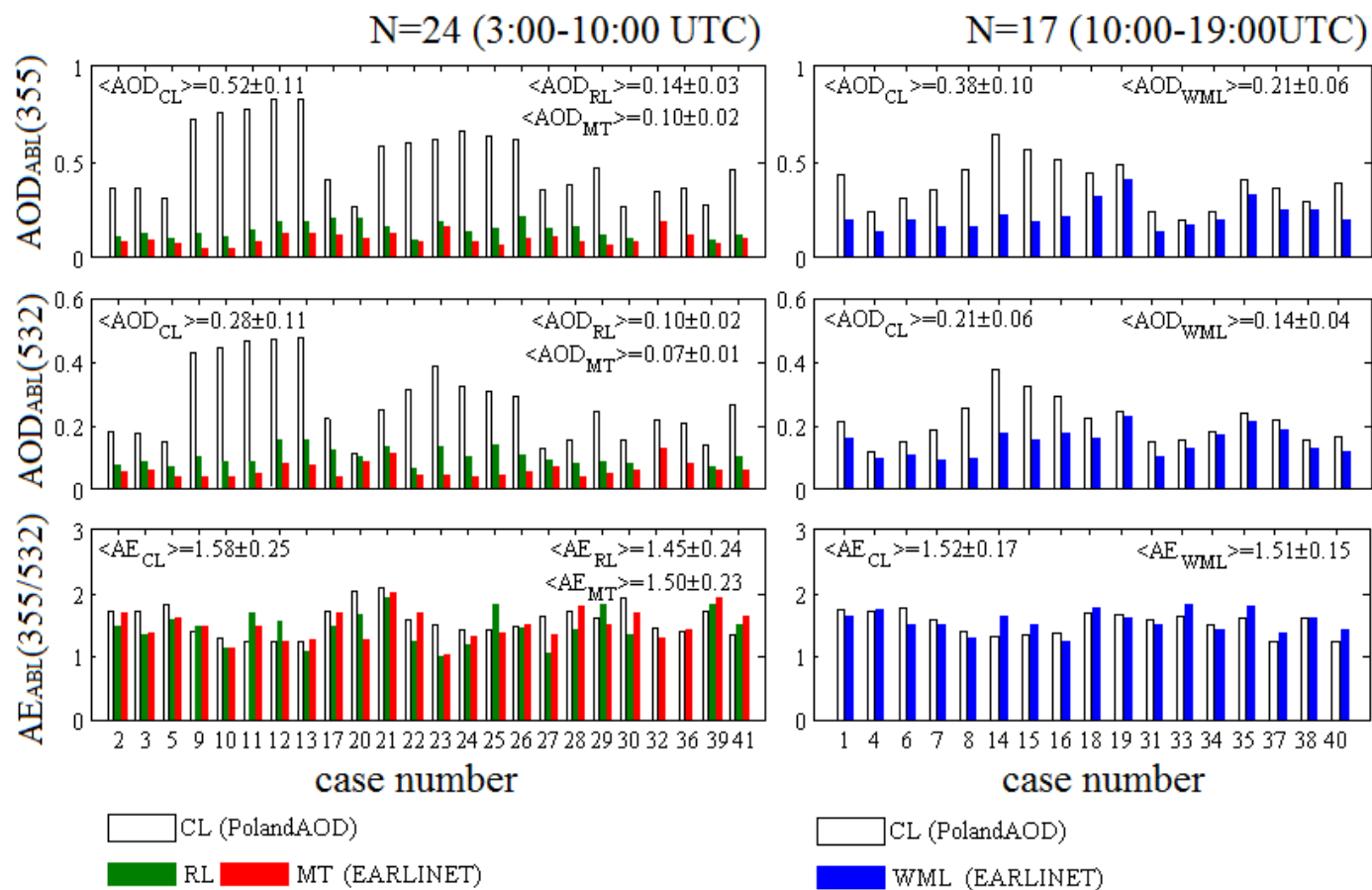
Figure 4. Hourly averages of aerosol optical depth (AOD) and Ångström exponent (ÅE) derived within the atmospheric boundary layer at 355 and 532 nm from PollyXT lidar at the EARLINET/ACTRIS site in Warsaw plotted along with the corresponding MFR-7 shadowband radiometer at the PolandAOD-NET site in Warsaw for July-September 2013, 2015, 2016 (leap year). Those were collocated measurements at the RS-Lab in Warsaw. AOD_{CL} of MFR-7 measurements at 415 and 500 nm were scaled to 355 and 532 nm using Ångström law.
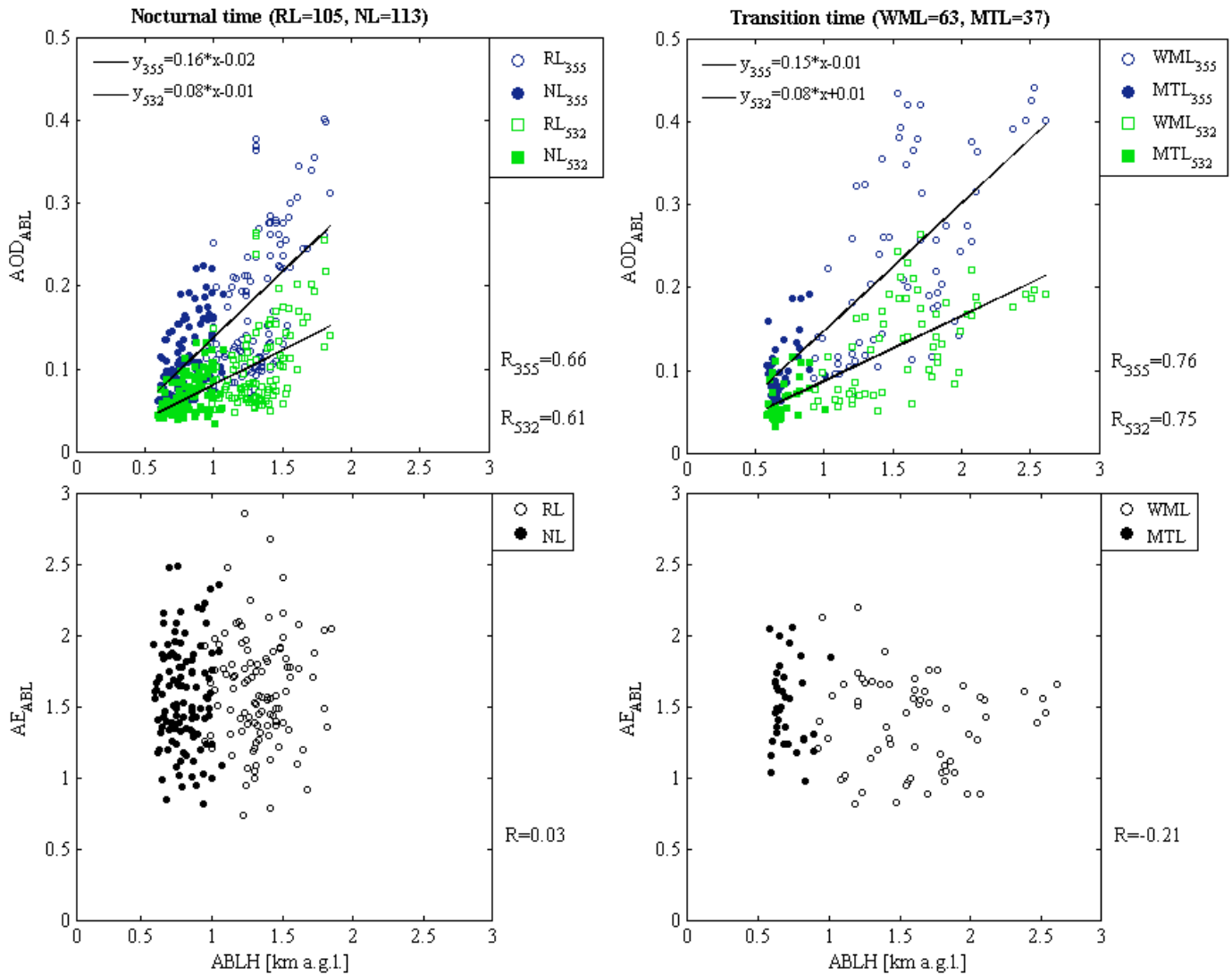
5   **Figure 5. Hourly averaged aerosol optical depth (AOD) and Ångström exponent (ÅE) derived within boundary layer at 355 and 532 nm versus atmospheric boundary layer height (ABLH), all derived from PollyXT lidar at the EARLINET/ACTRIS site of RS-Lab in Warsaw for July-September of 2013, 2015, 2016. Linear fit to data points is shown for correlation coefficients R > 0.6.**
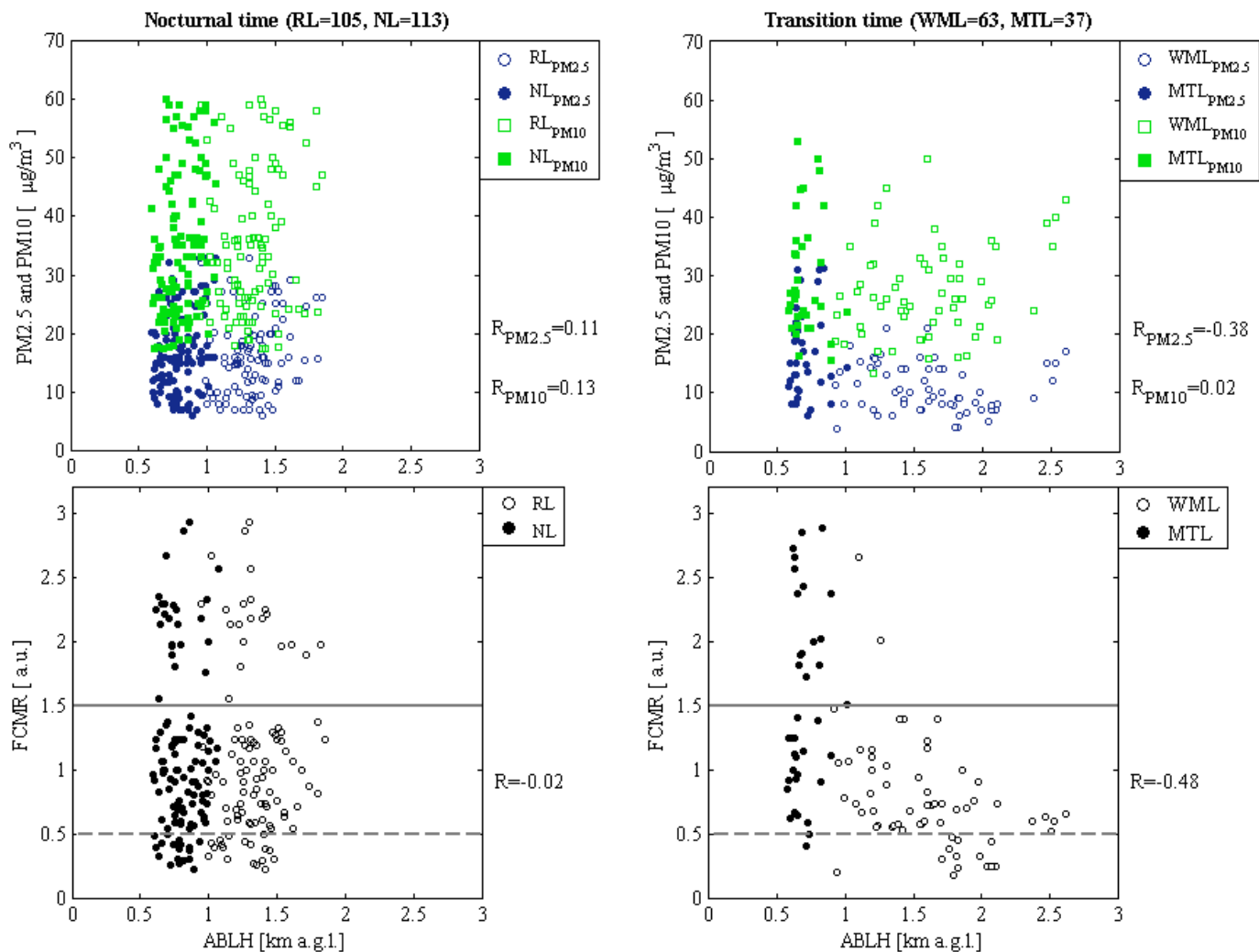
Figure 6. Hourly averages of surface fine to coarse mass ratio (FCMR), and particulate matter (PM$_{2.5}$ and PM$_{10}$) measured at the WIOS site in Warsaw-Ursynow versus atmospheric boundary layer height (ABLH) derived from PollyXT lidar at the EARLINET/ACTRIS site of RS-Lab in Warsaw for period of July-September of 2013, 2015, 2016. Thresholds of FCMR are marked as horizontal lines.
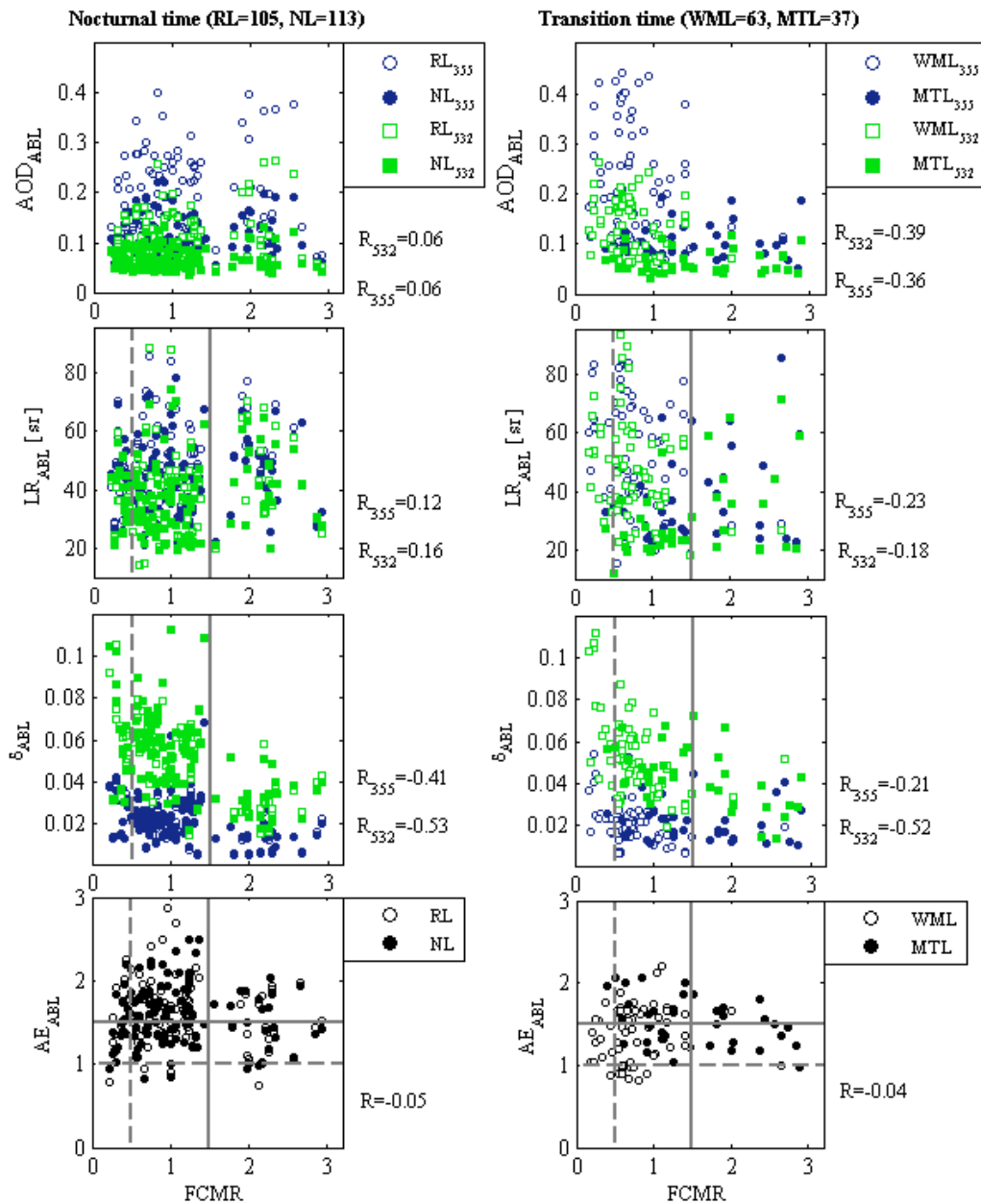
Figure 7. Hourly averaged aerosol optical depth (AOD), lidar ratio (LR), linear particle depolarization ratio (δ) and Ångström exponent (ÅE) derived within atmospheric boundary layer at 355 and 532 nm of PollyXT lidar at the EARLINET/ACTRIS site of RS-Lab in Warsaw for July-September of 2013, 2015, 2016 versus surface fine to coarse mass ratio (FCMR) derived from particulate matter (PM$_{2.5}$ and PM$_{10}$) measured at the WIOS site in Warsaw-Ursynow. Thresholds of ÅE and FCMR are marked as horizontal and vertical lines, respectively.
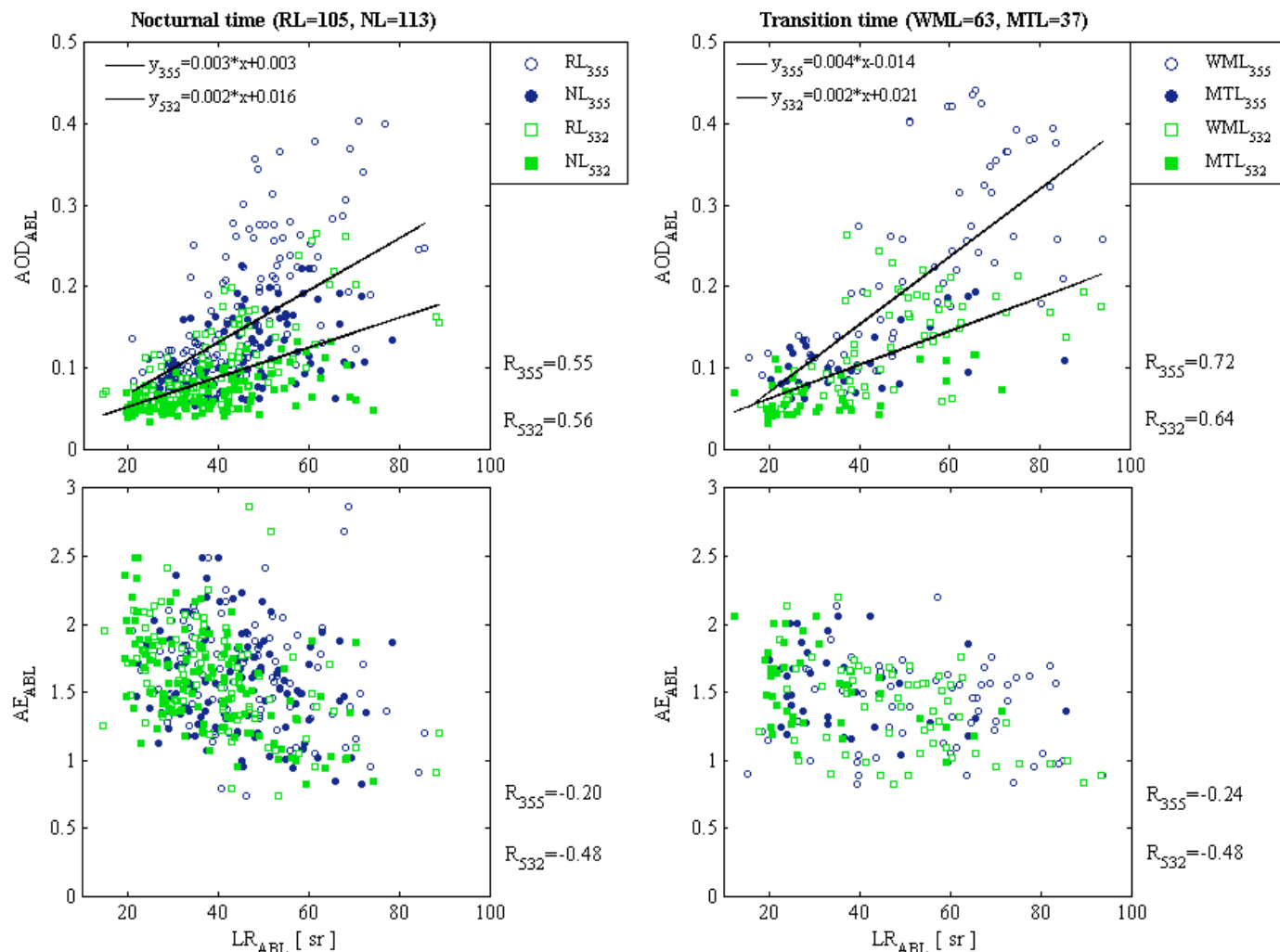
Figure 8. Hourly averaged aerosol optical depth (AOD), Ångström exponent (ÅE), and lidar ratio (LR) derived within atmospheric boundary layer at 355 and 532 nm from PollyXT lidar at the EARLINET/ACTRIS site of RS-Lab in Warsaw for period of July-September of 2013, 2015, 2016. Lack of correlation between linear particle depolarization ratio (δ) and lidar ratio (LR) is not shown for brevity. Linear fit to data points is shown for correlation coefficients R > 0.6.
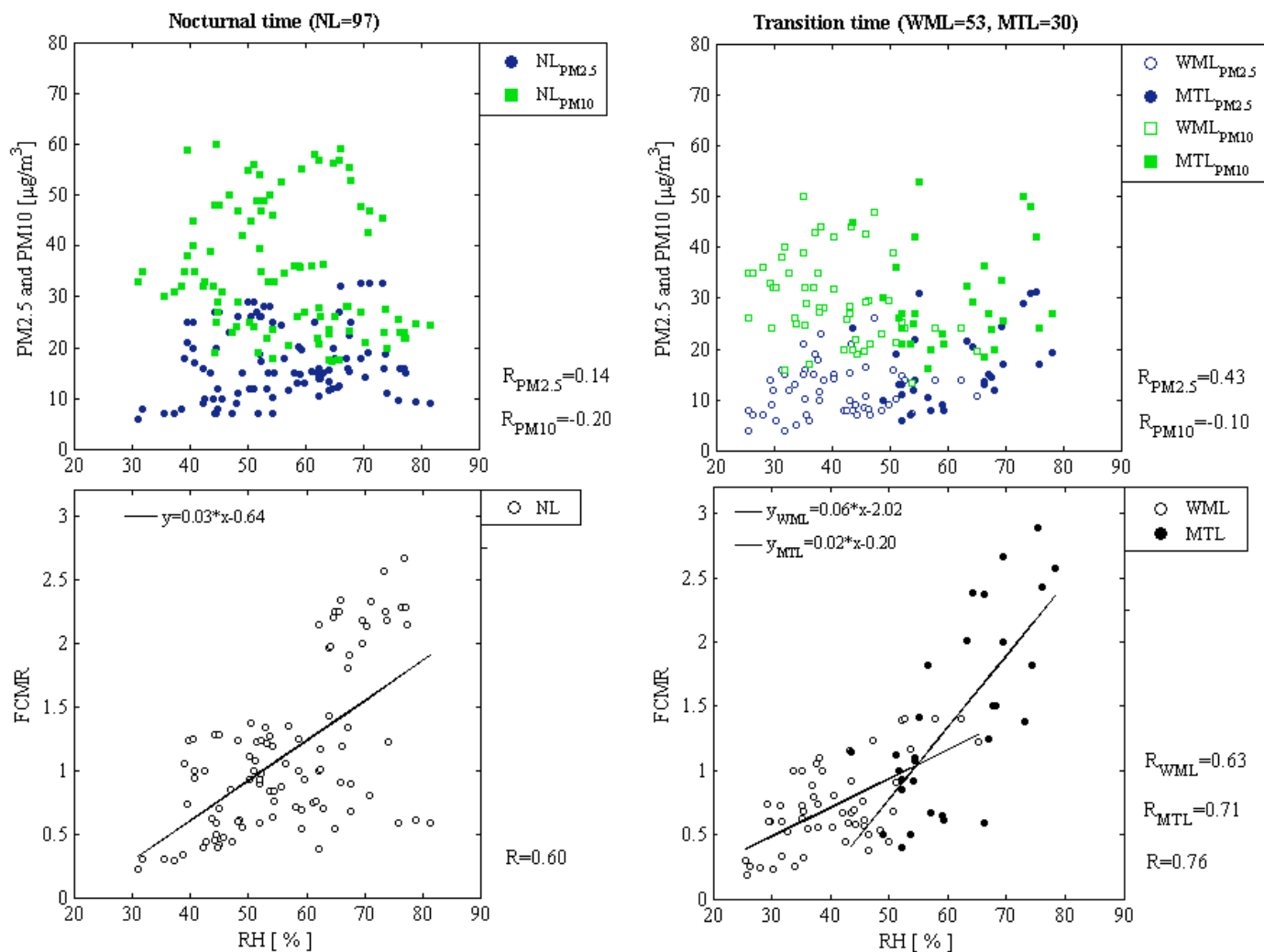
Figure 9. Hourly averaged near-surface relative humidity (RH) measured by the weather transmitter WXT510 (Vaisala) at RS-Lab in Warsaw for period of July-September of 2013, 2015, 2016 versus surface particulate matter PM$_{2.5}$ and PM$_{10}$ measured at the WIOS site in Warsaw-Ursynow. Linear fit to data points is shown for correlation coefficients R > 0.6.
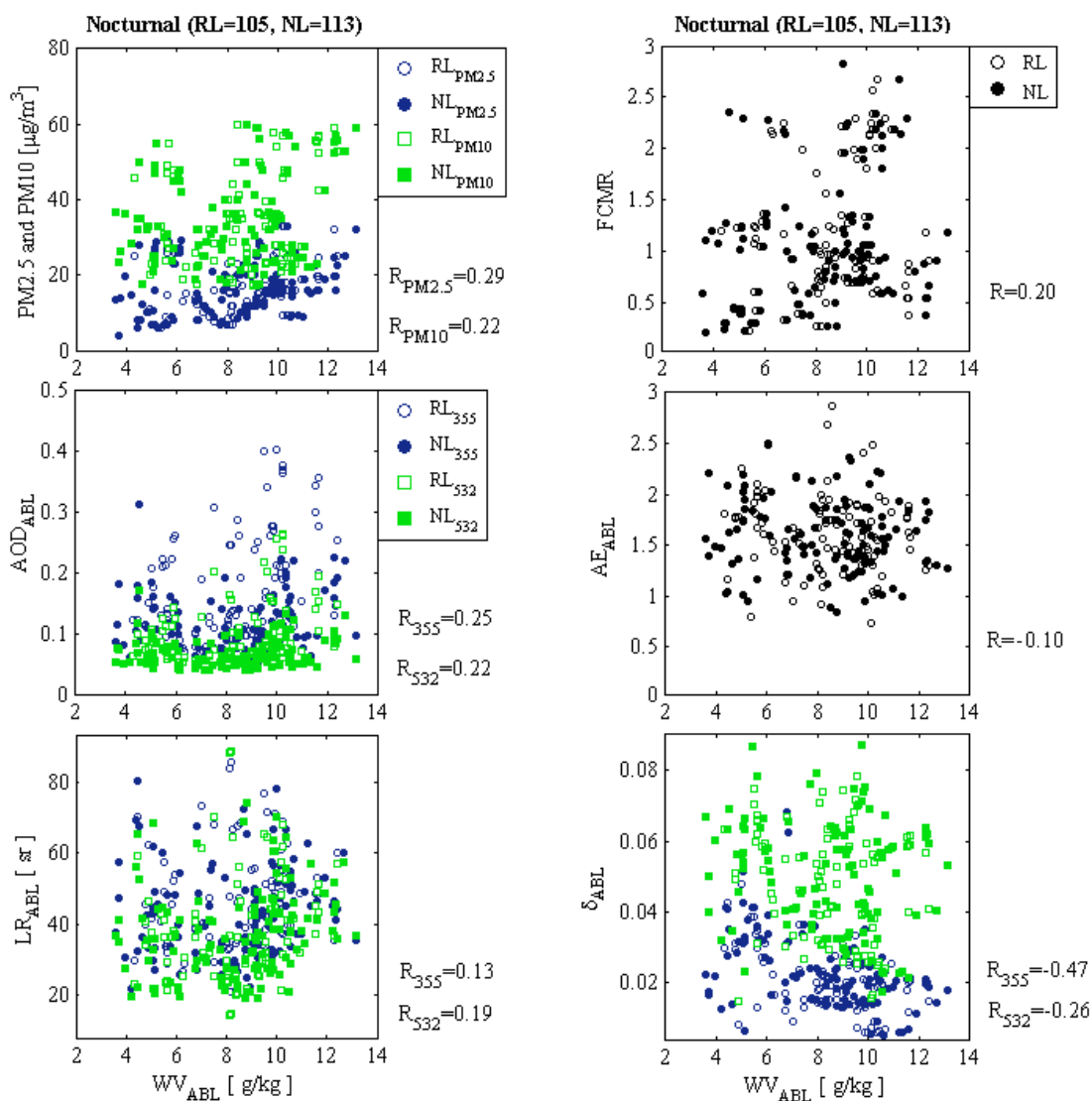
Figure 10. Nighttime hourly averaged water vapour mixing ratio (WV) versus aerosol optical depth (AOD), lidar ratio (LR), Ångström exponent (ÅE) and linear particle depolarization ratio (δ), all derived within atmospheric boundary layer form PollyXT lidar at the

5 **EARLINET/ACTRIS site of RS-Lab in Warsaw, and versus fine to coarse mass ratio (FCMR) and surface particulate matter PM$_{2.5}$ and PM$_{10}$ measured at the WIOS site in Warsaw-Ursynow, during period of July-September of 2013, 2015, 2016. Note that lidar-dervied WV is available only at nighttime.**
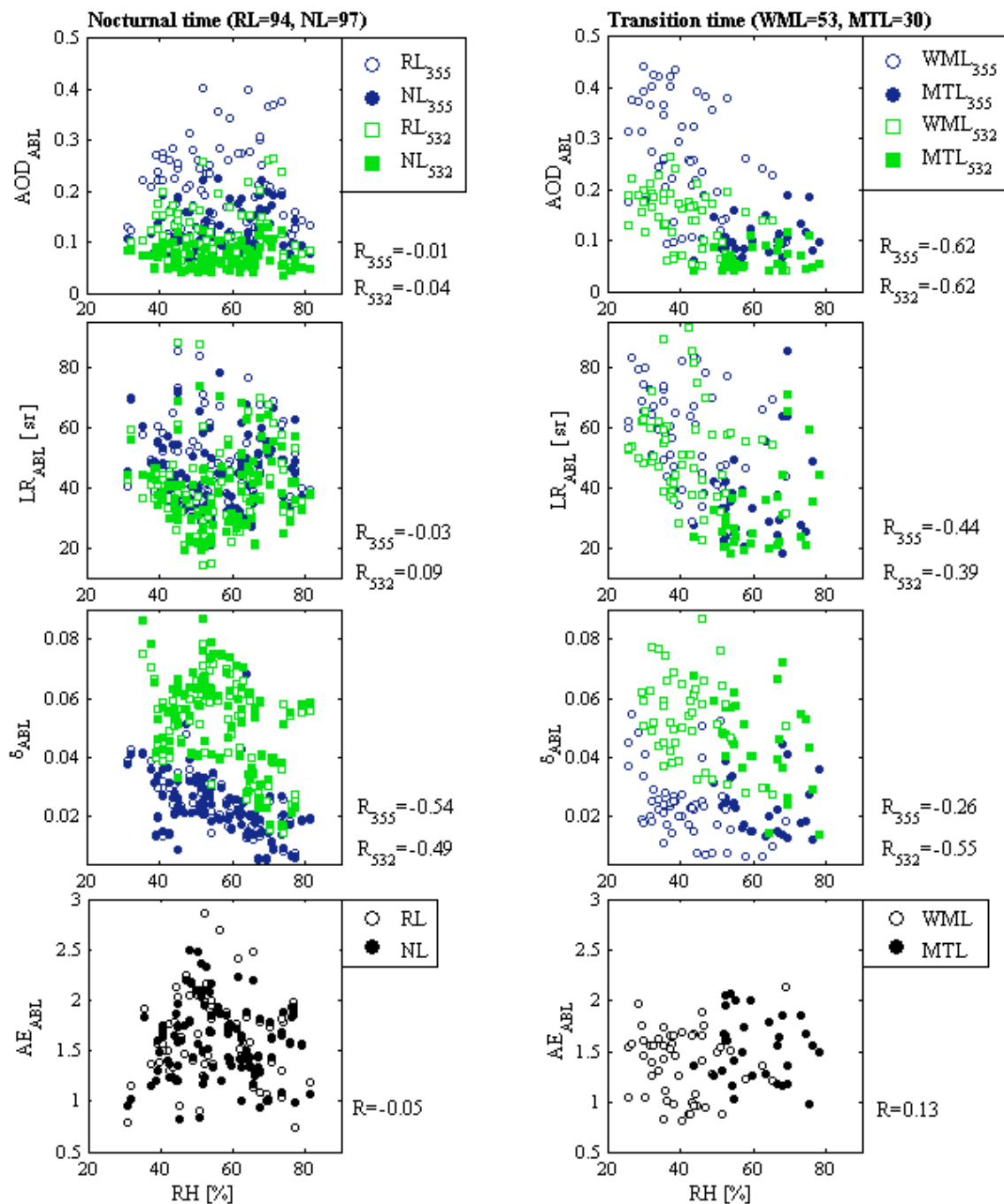
Figure 11. Hourly averaged near-surface relative humidity (RH) measured by the weather transmitter WXT510 (Vaisala) at RS-Lab in Warsaw versus aerosol optical depth (AOD), lidar ratio (LR), linear particle depolarization ratio (δ) and Ångström exponent (ÅE) derived within boundary layer at 355 and 532 nm from PollyXT lidar at the EARLINET/ACTRIS site of RS-Lab in Warsaw for period of July-September of 2013, 2015, 2016.